

# Radio Observations of the Hubble Deep Field South Region III: The 2.5, 5.2 and 8.7 GHz Catalogues and Radio Source Properties.

Minh T. Huynh

*Spitzer Science Center, MC220-6, California Institute of Technology, Pasadena CA 91125,  
USA*

`mhuynh@ipac.caltech.edu`

Carole A. Jackson

*Australia Telescope National Facility, CSIRO Radiophysics Laboratory, PO Box 76,  
Epping, NSW 2121, Australia*

Ray P. Norris

*Australia Telescope National Facility, CSIRO Radiophysics Laboratory, PO Box 76,  
Epping, NSW 2121, Australia*

## ABSTRACT

Deep radio observations of a wide region centred on the Hubble Deep Field South have been performed, providing one of the most sensitive set of radio observations acquired on the Australia Telescope Compact Array to date. A central rms of  $\sim 10\mu\text{Jy}$  is reached at four frequencies (1.4, 2.5, 5.2 and 8.7 GHz). In this paper the full source catalogues from the 2.5, 5.2 and 8.7 GHz observations are presented to complement Paper II, along with a detailed analysis of image quality and noise. We produce a consolidated catalogue by matching sources across all four frequencies of our survey. Radio spectral indices are used to investigate the nature of the radio sources and identify a number of sources with flat or inverted radio spectra, which indicates AGN activity. We also find several other interesting sources, including a broadline emitting radio galaxy, a giant radio galaxy and three Gigahertz Peaked Spectrum sources.

*Subject headings:* catalogs — surveys — radio continuum: galaxies

## 1. Introduction

Deep radio surveys over the last decade have pointed to the presence of a new population of radio sources distinct from classical radio galaxies and QSOs. These sources start to dominate the count for  $S_{1\text{GHz}} \lesssim 1$  mJy and they are responsible for the flattening in the source count for sub-mJy levels. Many different schemes have been put forward to explain this ‘excess’ of faint radio sources, including a non-evolving population of local ( $z < 0.1$ ) low luminosity radio galaxies (Wall et al. 1986), strongly evolving normal spirals (Condon 1984, 1989) and starburst galaxies (Windhorst et al. 1985; Rowan-Robinson et al. 1993). The sub-mJy radio source population is now thought to be a mix of low luminosity AGN, normal spirals and ellipticals, as well as starbursts, but surprisingly little is known about the exact nature of the faint radio population and the sources which dominate. This is because sub-mJy radio sources have faint optical counterparts and hence obtaining complete optical identifications has been historically difficult.

To help alleviate the significant time overheads of optical followup, we have targeted the Hubble Deep Field South (HDFS). This is a very well-studied field with publicly available data ranging in wavelengths from radio to UV-optical. The Hubble Space Telescope has observed this field to about 30th magnitude in the optical (Casertano et al. 2000), and similar depths in UV (Gardner et al. 2000) and NIR (Yahata et al. 2000). In addition to the main deep fields, the HST imaged nine Flanking Fields to a depth of  $I(\text{F814W}) \sim 26$ . From the ground, wide field imaging is available for an area  $44 \times 44$  arcmin in extent around the HDFS, which reaches about 25th magnitude in UBVRI (Teplitz et al. 2001). Spectroscopy has been obtained on the VLT for 194 targets in the main HDFS and Flanking Fields, resulting in reliable redshifts for 97 galaxies (Sawicki & Mallén-Ornelas 2003). Photometric redshifts are also available for thousands of galaxies in the HDFS and surrounding regions (Teplitz et al. 2001; Rudnick et al. 2001; Labbé et al. 2003), which have typical errors  $\delta z / (1 + z) \lesssim 0.1$ .

Radio observations of the HDFS were made between 1998 and 2001 with the Australia Telescope Compact Array (ATCA) using all four available frequency bands. Between 100 to 300 hours of observing at each band yielded images at 1.4, 2.5, 5.2 and 8.7 GHz with maximum sensitivities of  $\sim 10 \mu\text{Jy}$  rms. A detailed description of the observations, data reduction, and initial results was given by Norris et al. (2005) (hereafter Paper I). The full 1.4 GHz catalogue, a detailed 1.4 GHz image analysis and radio source count was presented in Huynh et al. (2005) (hereafter Paper II).

The advantage of the ATHDFS dataset over other deep radio surveys is that it is at four frequencies, making it possible to do an analysis of the radio spectra of the individual sources and identify those with spectra characteristic of AGN. This paper details the 2.5, 5.2 and 8.7 GHz catalogue and an analysis of the radio spectral properties of sources in the

ATHDFS.

This paper is outlined as follows. We summarise the the 2.5, 5.2 and 8.7 GHz observations and data reduction in Section 2. A detailed analysis of the images at these three frequencies is discussed in Section 3, and the catalogues listed in Section 5. We present a consolidated catalogue in Section 6 where radio sources have been matched across all four ATHDFS bands. Section 7 presents an analysis of the radio spectral index of ATHDFS sources and other interesting radio sources are discussed in Section 8.

We assume a Hubble constant of  $71 \text{ km s}^{-1} \text{ Mpc}^{-1}$ ,  $\Omega_{\text{M}} = 0.27$  and  $\Omega_{\Lambda} = 0.73$  throughout this paper.

## 2. Observations and Data Reduction

Here we provide a brief summary of the 2.5, 5.2 and 8.7 GHz observations and data reduction which are discussed in detail in Paper I. The observations consist of single pointings centred on RA = 22h 33m 25.96s and Dec =  $-60^{\circ} 38' 09.0''$  (J2000) (2.5 GHz), and RA = 22h 32m 56.22s and Dec =  $-60^{\circ} 33' 02.7''$  (J2000) (5.2 and 8.7 GHz). The 5.2 and 8.7 GHz observations are centred on the HST WFPC field, while the 2.5 GHz observations were pointed halfway between the WFPC field and a bright confusing source to allow the bright source to be well cleaned from the 2.5 GHz image.

We used a wide variety of ATCA configurations to maximise  $uv$  coverage. The correlator was set to continuum mode ( $2 \times 128$  MHz bandwidth), with each 128 MHz bandwidth divided into  $32 \times 4$  MHz channels. The primary flux density calibrator is PKS B1934-638, while secondary gain and phase calibrations were taken throughout our observations using both PKS B2205-636 and PKS B2333-528.

The 2.5 and 5.2 GHz images contained sidelobes from off-field sources. The image sensitivity was improved by removing the clean components of these off-field sources before the final imaging. The 2.5 GHz image was also improved with one iteration of phase and amplitude self-calibration. The 5.2 and 8.7 GHz data were of sufficient quality that self-calibration was not needed.

## 3. Analysis of 2.5, 5.2 and 8.7 GHz Images

The parameters of the final ATHDFS images are summarised in Table 1. The 1.4 GHz values are included for completeness. For each frequency we list the pointing (J2000), number

of effective hours observed, and synthesised beam (size and position angle). The rms noise at the image centre is also given, along with the value of the most negative pixel.

### 3.1. Clean Bias

If  $uv$  coverage is poor, the cleaning process can redistribute flux from real sources on to noise peaks. Our  $uv$  coverage is good, and in Paper II we found that clean bias was small at 1.4 GHz. Here we perform a similar test on the 2.5, 5.2 and 8.7 GHz images.

To perform the clean bias check, point sources are injected random positions in the data before cleaning, and the data cleaned to the same level as the final images. Source peak fluxes before and after cleaning were then compared. We injected 40 sources at  $5\sigma$ , 15 at  $6\sigma$ , 15 at  $7\sigma$ , 15 at  $8\sigma$ , 15 at  $9\sigma$ , 10 at  $10\sigma$ , 3 at  $20\sigma$ , 2 at  $30\sigma$ , 1 at  $50\sigma$  and 1 at  $100\sigma$ . This simulation was repeated 50 times to get reliable number statistics.

Figure 1 shows the result of our clean bias check. The average source flux measured after the cleaning process ( $S_{\text{output}}$ ) divided by the true source flux ( $S_{\text{input}}$ ) is shown for the various values of input source signal-to-noise ( $S_{\text{input}}/\sigma_{\text{local}}$ ). It is evident that clean bias only affects the faintest sources.

An analytical form of the clean bias effect was obtained by a least squares fit to the function

$$S_{\text{output}}/S_{\text{input}} = a + b \frac{1}{S_{\text{input}}/\sigma_{\text{local}}}.$$

The best fit values for  $a$  and  $b$  are shown in Table 2. The resulting best fit curves are plotted as solid lines in Figure 1.

### 3.2. Bandwidth Smearing

Bandwidth smearing is a well-known effect caused by the finite width of the receiver channels. This aberration reduces the peak flux density of a source while correspondingly increasing the size of a source such that the integrated flux density is conserved. In Paper II we found that the 1.4 GHz image is affected by bandwidth smearing, and at 20 arcmin from the phase centre, which is the 1.4 GHz catalogue limit, sources are attenuated by  $\sim 18\%$ .

We calculate the bandwidth smearing attenuation for the 2.5, 5.2 and 8.7 GHz images using the appropriate beam parameters and Equation 1 from Paper II. Since bandwidth smearing is inversely proportional to frequency we expect the attenuation to be lower at

these higher frequencies than at 1.4 GHz. The bandwidth smearing as a function of distance from the centre for the three images are shown in Figure 2. The dashed lines in Figure 2 indicate the maximum distance at which sources are catalogued. We find bandwidth smearing is at most 5% in the 2.5 GHz image, and negligible at the two higher frequencies.

### 3.3. Noise Maps

To investigate the noise characteristics of our images, and eventually obtain catalogues based on the local signal to noise ratio (SNR), we construct noise maps. Noise maps which contain the pixel by pixel root mean square (rms) noise distribution of each of the ATHDFS images were made using the SExtractor package (Bertin & Arnouts 1996). SExtractor has been found to be to be reliable for radio images (Paper II, Bondi et al. 2003).

As for Paper II, we ran SExtractor on the ATHDFS images with a mesh size set to  $8 \times 8$  beams. Grey scale images of the SExtractor noise maps are shown in Figure 3. The noise is lowest in the centre and increases with radial distance, as expected from single-pointing observations which are dominated by primary beam effects. Figure 4 shows the average noise as a function of distance from the centre for the three ATHDFS noise maps. This increase in noise is roughly a parabolic shape due to the primary beam attenuation. Histograms of the pixel values of each noise map are shown in the Figure 5. The distributions peak at a value of about  $10 \mu\text{Jy}$ , but have large wings at high noise values due to the radially increasing noise.

In Paper II we found regions of increased noise around bright sources. The 2.5 GHz noise map clearly shows increased noise around the brightest ( $S_{2.5\text{ GHz}} = 112 \text{ mJy}$ ) source, although the dynamic range problem is not as large here as for 1.4 GHz. The area around this bright confusing source has noise which is up to a factor of 2 greater than the nearby unaffected region. This can be seen as the noise bump at approximately 6 arcmin from the 2.5 GHz image centre. The noise in the 5.2 and 8.7 GHz images is unaffected by bright sources.

## 4. Source Extraction at 2.5, 5.2 and 8.7 GHz

A sensible maximum radial distance for the source cataloging has been determined, accounting for the following factors: i) the radial noise distribution, ii) the primary beam attenuation, and iii) the bandwidth smearing effect. The dominant effect at 2.5, 5.2 and 8.7 GHz is the primary beam attenuation. Similar to Paper II for 1.4 GHz, we catalogue to the

40% response level of the primary beam. Thus the maximum radial distances are 12, 5.5 and 3.5 arcmins for the 2.5, 5.2 and 8.7 GHz images, respectively. As mentioned in Section 3.2, this results in bandwidth smearing of only 5% *at worst* for sources at the edge of the 2.5 GHz catalogued region.

Signal-to-noise maps are generated by dividing the original radio maps by the SExtractor noise map. The *MIRIAD* task *IMSAD* was then used to derive a preliminary list of source “islands” with a peak flux density level of at least  $4\sigma$ . This task searches for “islands” of pixels above a cutoff, set here to  $4\sigma$ , and attempts to fit gaussian components to the “islands”. This resulted in 258, 80 and 36 source “islands” extracted at 2.5, 5.2 and 8.7 GHz, respectively.

To derive source flux densities and sizes, we fit each source “island” found by *IMSAD* with an elliptical Gaussian. All sources were visually inspected for obvious failures and poor fits. A reference peak value was derived using the (*MIRIAD* interpolation task *maxfit*), and the Gaussian fit was considered good if the difference between the fitted peak and reference peak was less than 20% of the reference value and the fitted position was inside the  $0.9S_{\text{peak}}$  flux density contour. We compared the Gaussian integrated fluxes to fluxes directly measured from summing pixels greater than  $3\sigma$  in the source area. In many cases the Gaussian fit provided good values for the position and peak flux densities but not for integrated flux densities. These sources are flagged with “2” in the catalogue.

The reliability of the sources was estimated by running source extraction on the negative images. This is a valid estimate provided the cleaning process didn’t add extra negative or positive peaks on to the images. As described in Paper I, the clean model residuals were monitored and the cleaning process was stopped when there was no reduction from extra components. So we expect that the cleaning process didn’t add many positive or negative peaks. Table 3 summarizes the results of running source extraction on the negative image. At  $5\sigma$  the 5.2 and 8.7 GHz catalogues have over 96% reliability. At 2.5 GHz we have enough statistics to examine the  $5 - 5.5\sigma$  sources, and find that these are only about 40% reliable. With a SNR greater than  $5.5\sigma$  the 2.5 GHz catalogue would have about 99% reliability. We thus cut off the catalogues at  $5.5\sigma$ ,  $5\sigma$  and  $5\sigma$  at 2.5, 5.2 and 8.7 GHz. The final catalogues have 71, 24 and 6 sources at 2.5, 5.2 and 8.7 GHz, respectively.

Given a prior 1.4 GHz position, it maybe feasible to push the detection limit lower than  $5\sigma$ . We searched for low SNR sources by matching  $3 - 5\sigma$  sources which lie within  $2\sigma$  positional uncertainty of a 1.4 GHz source. The positional uncertainty was determined by adding the average 1.4 GHz uncertainty (1.1 arcsec) in quadrature with the positional uncertainty of a  $3\sigma$  source. At 2.5 GHz the allowed positional offset is 3.8 arcsec, and for 5.2 and 8.7 GHz it is 2.8 arcsec. Thus, there are 71, 18, and 2 sources at 2.5, 5.2 and 8.7

GHz, respectively, which are low SNR high frequency counterparts to 1.4 GHz sources. We include these sources in supplementary catalogues. To test the reliability of the low SNR supplementary catalogues, we shifted the 1.4 GHz positions by 0.5 arcmin and repeated the matching of  $3 - 5\sigma$  sources. As a result, we estimate that 4/71 (6%) of the low SNR 2.5 GHz sources are false, and no false low SNR sources were found at 5.2 and 8.7 GHz.

## 5. Catalogues at 2.5, 5.2 and 8.7 GHz

The main catalogues for the three frequencies are presented in Tables 4 to 6. These are independent, statistically complete and reliable catalogues for each frequency. We also include supplementary catalogues for each frequency (Tables 7 and 8). The supplementary catalogues contain low SNR sources which have a priori 1.4 GHz positions.

A description of the Tables is as follows.

*Column (1)* — Source ID. The ID numbering for the supplementary catalogues starts from the end of the main catalogues.

*Column (2)* — Right Ascension in J2000.

*Column (3)* — One sigma uncertainty of Right Ascension, in arcsec.

*Column (4)* — Declination in J2000.

*Column (5)* — One sigma uncertainty of Declination, in arcsec.

*Column (6)* — Source peak flux density, in mJy. The values given here are not corrected for the systematic effects described in Section 3. ATCA fluxes are generally estimated to be accurate to about 10%.

*Column (7)* — Source integrated flux density, in mJy.

*Column (8) and (9)* — The *deconvolved* major and minor axes (FWHM) of the source,  $\Theta$ , in arcsec. Only given for successfully deconvolved sources.

*Column (10)* — The *deconvolved* position angle (PA, measured from N through E) of the source, in degrees. Only given for successfully deconvolved sources.

*Column (11)* — The signal-to-noise ratio of the detection, calculated as *IMRAD* fitted peak/ $\sigma_{\text{local}}$ .

*Column (12)* — Gaussian fit flags : “2” refers to poor integrated flux density, see Section 4 for more details.

## 6. Combining the ATHDFS Catalogues

Including the 1.4 GHz catalogue from Paper II, we have catalogues at four radio frequencies. The four images have similar sensitivities, but different area coverages. We now combine these independent catalogues into one consolidated catalogue which lists the flux densities at all frequencies for each individual radio source.

We start by matching the positions of the sources in the 1.4 GHz catalogue (Paper II) against all source positions in the three higher frequency catalogues. The allowable offset was set to  $3\sigma$ , i.e. 3 times the positional uncertainties in the catalogues (added in quadrature). This results in a total of 499 individual sources comprising:

- the 466 1.4 GHz sources, as presented in Paper II,
- 11 unmatched 2.5 GHz sources,
- 5 unmatched 5.2 GHz sources,
- 4 unmatched 8.7 GHz sources.

Each of the 486 sources from this first pass was inspected for missed matches. The simple  $3\sigma$  positional cutoff missed bona fide matches due to a variety of reasons, including:

1. the positional errors being smaller than the image cellsize, and hence the allowable offset was too small, and
2. individual sources at 1.4 GHz catalogued as multiple sources at higher frequencies and resolution.

After inspection we find that only five 2.5 GHz sources and two 8.7 GHz sources remain un-matched to sources in the 1.4 GHz catalogue. The final consolidated catalogue contains 473 individual sources.

The consolidated catalogue is presented in Table 9. It includes information from the supplementary catalogues. Flux density upper limits (assuming point sources) are listed for 1.4 GHz sources without counterparts at the higher frequencies, if they lie in the catalogued region at that frequency.

Table 9 is organised as follows.

*Column (1)* — Source name.



*Column (2)* — Right Ascension in J2000.

*Column (3)* — Declination in J2000.

*Column (4)* — Coordinate flag indicating the frequency from which the source coordinates are obtained. “L” indicates 1.4 GHz, “S” indicates 2.5 GHz, “C” indicates 5.2 GHz, and “X” indicates 8.7 GHz.

*Column (5)* — Source 1.4 GHz flux density, in mJy.

*Column (6)* — Source 2.5 GHz flux density, in mJy. Flux densities from low SNR sources in the supplementary catalogue are listed in brackets. A “-” indicates the source lies outside the catalogued region.

*Column (7)* — Source 5.2 GHz flux density, in mJy. Flux densities from low SNR sources in the supplementary catalogue are listed in brackets. A “-” indicates the source lies outside the catalogued region.

*Column (8)* — Source 8.7 GHz flux density, in mJy. Flux densities from low SNR sources in the supplementary catalogue are listed in brackets. A “-” indicates the source lies outside the catalogued region.

*Column (9)* — The spectral index between 1.4 and 2.5 GHz, ( $S \propto \nu^\alpha$ ).

*Column (10)* — The spectral index between 2.5 and 5.2 GHz, ( $S \propto \nu^\alpha$ ).

*Column (11)* — The spectral index between 5.2 and 8.7 GHz, ( $S \propto \nu^\alpha$ ).

*Column (12)* — AGN flag, see Section 7.

Note that the flux densities in this catalogue are peak flux densities for sources undeconvolved at that particular frequency, otherwise integrated flux densities are presented. The radio spectral indices are discussed in the following section.

## 7. Radio Spectral Indices

Spectral indices for our sources cannot be obtained from the original catalogues since the resolution of the images differ between the frequencies. In particular, low surface brightness regions that are detected in the low resolution 1.4 GHz image may be resolved out at higher frequencies.

We therefore produced low resolution images at 2.5, 5.2 and 8.7 GHz by imaging only the  $uv$  data that was equal to, or less than, the highest resolution  $uv$  point in the 1.4 GHz

image ( $6\text{km}/20\text{cm} = 30k\lambda$ ). The resulting images are of similar resolution to the 1.4 GHz image. Flux density measurements from these low resolution images were made and the resulting spectral indices for sources detected at more than one frequency are given in Table 9. The upper limit to  $\alpha_{1.4\text{GHz}}^{2.5\text{GHz}}$  is also given for 1.4 GHz sources that lie within the 2.5 GHz catalogued region.

The distribution of the spectral indices is plotted in Figures 6 to 8. The peak in the distribution of the spectral index  $\alpha_{1.4\text{GHz}}^{2.5\text{GHz}}$  ( $S \propto \nu^\alpha$ ) is  $-0.5$ . This is close to, but flatter than, the canonical value of  $-0.8$  expected for radio synchrotron emission (Condon 1992). This is because the spectral indices plotted here are only for ATHDFS sources detected at both frequencies, which introduces a bias towards flatter sources. Many steep spectrum 1.4 GHz sources are not detected at 2.5 GHz because the images have similar rms sensitivities. The alpha upper limit is shown in Figure 9, which indicates we can not detect faint ( $S_{1.4\text{GHz}} \lesssim 0.06$  mJy) sources with  $\alpha_{1.4\text{GHz}}^{2.5\text{GHz}} \lesssim 0$  at 2.5 GHz.

The mean spectral index  $\alpha_{1.4\text{GHz}}^{2.5\text{GHz}}$  for all sources including the supplementary 2.5 GHz detections is  $-0.54 \pm 0.25$ . The mean spectral index of the 2.5 GHz selected sample ( $S_{2.5\text{GHz}} > 5.5\sigma$ ) is  $-0.39 \pm 0.17$ . This is consistent with previous work which finds that samples selected at higher frequency have flatter spectral indices (e.g Windhorst et al. 1993; Prandoni et al. 2006).

In Figure 9 we show the spectral indexes as a function of 1.4 GHz flux density for 136 sources in both the 1.4 GHz and 2.5 GHz catalogues. Our sample is complete to  $\sim 0.1$  mJy at both 1.4 GHz and 2.5 GHz and the mean spectral index,  $\alpha_{1.4\text{GHz}}^{2.5\text{GHz}}$ , for sources with  $0.1 < S_{1.4\text{GHz}} < 1$  mJy is  $-0.66 \pm 0.28$ , with a median value of  $-0.62$ . These values are consistent with the spectral indexes for bright samples at these flux densities (although between 1.4 and 5 GHz) (Prandoni et al. 2006). Whilst some authors have observed a flattening of the spectral index at the sub-mJy level (Windhorst et al. 1993; Prandoni et al. 2006), we have limited statistics to explore this regime.

### 7.1. Flat and Inverted Spectrum Sources

The spectral shape of a radio source can give clues to the physical source of the radio emission. For a homogeneous, optically thin synchrotron radio source with constant magnetic field strength  $B$ , the electron energies have a power law distribution of the form:

$$N(E) dE = N_0 E^s dE ,$$

and the spectral index  $\alpha = (s + 1)/2$ . The typical observed value of the spectral index is  $\langle \alpha \rangle = -0.7$ , so  $\langle s \rangle = -2.4$ , although this only applies at higher frequencies. At low

frequencies the emitting gas is optically thick and self-absorption becomes important. The radio spectra turns over to yield  $S \propto \nu^{2.5}$ , but the exact frequency of the turnover depends on many parameters, including the magnetic field strength  $B$  and electron density. In AGN, the spectral indices are close to flat but progressively steeper ( $\alpha < -1$ ) at higher radio frequencies. The flatness of the radio spectrum in AGN is attributed to the complex source structure, where the low frequency turnover is different for various components of the radio source (e.g. NRAO140; Marscher 1988). When the turnover frequency is high enough, it is possible to observe an inverted spectrum.

This flat or inverted spectrum cannot be produced by normal synchrotron emission from star formation processes. The spectral index of our radio sources therefore provides us with a diagnostic to identify AGNs in our sample. The uncertainty in the spectral index for faint sources becomes large at about  $S_{1.4\text{GHz}} < 0.5$  mJy (see Figure 9). We therefore use the following conservative classification scheme: if  $S_{1.4\text{GHz}} < 0.5$  mJy sources must have  $\alpha > 0$  to be classed as AGN, and brighter sources must have  $\alpha > -0.3$ . The 34 sources which are classed as AGN in this way are flagged as AGN in Table 9.

Three sources have been flagged as a subclass of AGN called Gigahertz Peaked Spectrum (GPS), because the spectrum is inverted between 1.4 and 2.5 GHz, but steep at higher frequency. This indicates that these sources may be young, extremely compact AGN (see, for example O’Dea et al. 1991; O’Dea 1998). The three GPS sources are discussed in detail in Section 8.3.

## 8. Discussion of Interesting Sources

### 8.1. Broadline Emitting Radio Galaxy

Classical radio galaxies have been classed morphologically into two types (Fanaroff & Riley 1974):

1. Fanaroff Riley class 1 (FRI) radio galaxies are AGN with radio jets that become more diffuse in regions distant from the galactic nucleus, and
2. Fanaroff Riley class 2 (FRII) radio galaxies are lobe dominated with bright emitting hot-spots in the outer region of their radio lobes.

There is a strong correlation of morphology with radio luminosity, as noted by Fanaroff & Riley (1974). For low frequencies (178 MHz), sources with radio luminosities greater than  $P = 2 \times 10^{25}$  W Hz<sup>-1</sup> sr<sup>-1</sup> are almost all FRII type, and lower luminosity sources are FRI

(Urry & Padovani 1995, and references therein). At GHz frequencies the luminosity ranges of the two classes overlap by a few decades. According to some unification schemes for radio loud AGN, BL Lac objects are FRI radio galaxies with jets aligned along the line of sight, and Flat Spectrum Radio Quasars (FSRQs) are FRII radio galaxies viewed in a similar way (Urry & Padovani 1995; Jackson & Wall 1999; Urry et al. 2002). Spectroscopically, the host of FRIs usually have weak, if any, narrow emission lines (Hine & Longair 1979; Laing et al. 1994). Most show a quiescent elliptical galaxy spectrum. In this sense, FRIs are thought to have no photo-ionizing flux, and the difference between FRIs and FRIIs is due to the different accretion processes present in these galaxies (e.g. Baum et al. 1995; Reynolds et al. 1996, but see Cao & Rawlings 2004).

The discovery of a FRI radio structure associated with a strong broad line emitting quasar E1821+643 is inconsistent with this paradigm. E1821+643 is an X-ray selected quasar serendipitously found to be associated with an FRI (Blundell & Rawlings 2001). Blundell & Rawlings (2001) suggest that FRI radio galaxies with quasar hosts have not been found previously due to the low sensitivity of older radio surveys, such as 3CRR, and the low space density of quasars. It was only after very deep radio imaging of this quasar was performed with the VLA that the FRI radio structure was revealed.

The deep ATHDFS survey presents a dataset to search for similar objects. We have discovered a radio galaxy similar to E1821+643: ATHDFS\_223319.1-604428. This radio galaxy is associated with a host galaxy which has optical magnitudes of  $V = 19.4$  and  $I = 18.1$ . A low resolution spectrum of this source was taken on the Anglo-Australian Telescope (AAT) with the 2dF fibre-fed spectrograph, as part of a broader program to obtain spectroscopic redshifts of radio sources in the ATHDFS. The spectrum obtained of ATHDFS\_223319.1-604428 is shown in Figure 10. We identify the broad feature ( $5000 \text{ km s}^{-1}$ ) at  $4620 \text{ \AA}$  as MgII 2799, which is consistent with the H and K Calcium absorption seen in the spectrum, giving a redshift of  $z = 0.65$ . Table 10 summarises the properties of ATHDFS\_223319.1-604428. The broad MgII line has a restframe measured equivalent width (EW) of  $45 \text{ \AA}$ . This is close to the MgII EW of  $50 \pm 8 \text{ \AA}$  found for QSOs in the Parkes quarter-Jansky flat-spectrum sample (Hook et al. 2003), indicating ATHDFS\_223319.1-604428 has a line emission strength similar to FSRQs.

Figure 11 shows the radio morphology of ATHDFS\_223319.1-604428. This source is dominated by radio emission from both the core and inner regions close to the core of the object. On this basis, and having detected weak radio lobes (Figure 11), we suggest this is a possible FRI class radio galaxy. However, the unresolved source to the north maybe an edge-leading hotspot, so the radio morphology is unclear. If the northern source is a hotspot then ATHDFS\_223319.1-604428 is a moderate redshift FRII with a typical optical host.

## 8.2. Giant Radio Galaxy

Giant radio galaxies are defined to be radio sources with a projected linear size greater than 1 Mpc. Giant radio galaxies are useful for studying the late stages of radio source evolution because they are thought to be old radio sources. They have been used to test orientation dependent unified schemes and to probe the intergalactic medium at different redshifts (e.g. Subrahmanyan et al. 1996). According to models of radio source evolution (e.g. Kaiser et al. 1997, Blundell et al. 1999), giant radio galaxies must be extremely old (typically older than  $10^8$  yr) and usually located in under-dense environments, as compared to smaller radio sources of comparable radio power (e.g. Kaiser & Alexander 1999).

Visually inspecting the 1.4 GHz image, we find a giant radio galaxy in the Hubble Deep Field South region which was not included in the original ATHDFS 1.4 GHz catalogue. This is because it lies 27 arcmin from the image centre, and the original catalogue only included sources out to 20 arcmin (see Paper II). This giant radio galaxy, ATHDFS\_223432.9-601239, has a fitted peak of  $S_{1.4\text{GHz}} = 2.8 \pm 0.2$  mJy and the core has an integrated flux density of  $16.4 \pm 1.2$  mJy. Some of the extended radio structure maybe resolved out in the full resolution 1.4 GHz image, so we produced a tapered image and find the integrated flux density in the low resolution image is 21 mJy. Contours of this source in both the full and low resolution image are shown in Figure 12.

The optical host galaxy is bright, with B mag = 17.68 and I mag = 14.95 (Teplitz et al. 2001). We summarise the properties of this giant radio galaxy in Table 11. A low resolution spectrum was taken of this object with the 2dF spectrograph in 2001. The spectrum is clearly that of a quiescent elliptical galaxy (Figure 13), as expected of a galaxy with an old stellar population. Fitting the absorption features, we find that this optical host is at a redshift of 0.121. At this redshift, the linear extent of 390 arcsec translates to a size of 0.83 Mpc and it has a 1.4 GHz radio power of  $10^{23.8}$  W Hz<sup>-1</sup>.

The core and lobes of this giant radio galaxy are individually detected at 853 MHz in the Sydney University Molonglo Sky Survey (SUMSS) survey (Bock et al. 1999). The core has an integrated flux density of 16.3 mJy at 853 MHz (Mauch et al. 2003). Hence, the source has a inverted spectral index  $\alpha_{853\text{GHz}}^{1.4\text{GHz}} = 0.51 \pm 0.21$ , as expected of an AGN.

## 8.3. Gigahertz Peaked Spectrum Sources

Gigahertz peaked spectrum (GPS) sources are compact, powerful radio sources with a well-defined peak in their spectra at around 1 GHz. GPS radio sources make up a significant fraction of the bright radio source population ( $\sim 10\%$ ), but their contribution at low flux

densities is not well known. The turnover in the SED of GPS sources at about a GHz is due to either synchrotron self-absorption (Mutel et al. 1985), free-free absorption (Bicknell et al. 1997) or absorption from induced Compton scattering (Kuncic et al. 1998).

GPS sources have linear sizes comparable to or smaller than their optical host galaxies. High resolution radio interferometric observations have revealed that GPS sources have double lobed morphology, like classical radio galaxies, but on smaller scales of  $\lesssim 1$  kpc (e.g. Stanghellini et al. 1997). Two explanations have been proposed to explain the compactness of these objects: 1) GPS sources are young unevolved radio sources (e.g. Fanti et al. 1995), and 2) GPS sources are confined by the interstellar medium of the host galaxy (e.g. O’Dea et al. 1991). The current evidence favours the youth scenario: there is no compelling evidence to suggest there is enough dense gas to confine GPS sources (Pihlstrom et al. 2003), the observed expansion speed of GPS hotspots ( $0.1 - 0.2c$ ) imply ages of  $10^3$  years if the lobes expand at constant velocity, and the synchrotron cooling time of the radiating electrons indicate ages of  $10^3 - 10^5$  years (Murgia et al. 1999).

In the ATHDFS we have identified three GPS radio sources, ATHDFS\_223327.6-603414, ATHDFS\_223323.2-603249. and ATHDFS\_223259.5-602810. These sources have an inverted SED between 1.4 and 2.5 GHz, and a steep SED at frequencies between 2.5 and 8.7 GHz. We do not have a detailed radio SED for these objects, but our observations constrain the turnover frequency to between 2 – 4 GHz. These sources are compact, but marginally resolved in the 2.5 GHz image, where they are detected at the highest SNR. They are unresolved in the higher resolution 5.2 and 8.7 GHz images, so they are probably not resolved at 2.5 GHz, but just fit with a slightly larger than point source Gaussian.

One GPS source, ATHDFS\_223259.5-602810, is not detected in ground-based CTIO imaging to I mag  $\sim 23$  (Teplitz et al. 2001), but this source lies near a bright star so optical photometry is uncertain. The other two sources lie within the HST flanking field observations, but are not detected. The HST flanking field observations reach a depth of I (F814W) mag = 26.0 (Lucas et al. 2003). Assuming the Hubble diagram found for GPS sources (O’Dea 1998, Drake et al. 2004) holds for these two GPS sources, a radio source with I mag = 26.0 is expected to lie at  $z \gtrsim 2$ . Assuming I mag  $> 26.0$  and neglecting K corrections, these sources are fainter than an absolute I (F814W) mag =  $-20.0$  at a redshift of  $z = 2$ . Results from the Sloan Digital Sky Survey (SDSS) have found that  $M_i^* = -21.26$  (Blanton et al. 2001), which corresponds to  $M_i^* = -21.77$  assuming the the conversion from the SDSS team <sup>1</sup>. GPS sources at redshifts  $z < 1$  are usually one to two magnitudes brighter than  $M^*$  (O’Dea 1998, Drake et al. 2004). This implies these two GPS sources are either

---

<sup>1</sup><http://www.sdss.org/dr4/algorithms/sdssUBVRITransform.html>

unusually faint in the optical, or are at  $z \geq 2$ .

#### 8.4. Ultra-Steep Spectrum Radio Sources

Tracing radio galaxies out to high redshift provides a way to study the formation and evolution of massive galaxies in the early universe. The well known Hubble  $K-z$  relation (e.g. Longair & Lilly 1984; De Breuck et al. 2002) is evidence that high  $z$  radio galaxies can be used as a tracer of the most massive star forming galaxies. Radio galaxies have now been found out to redshifts of 5.2 (De Breuck et al. 2000). One of the most successful ways to select high redshift radio galaxies (HzRGs) is by using the ultra steep spectrum (USS) selection technique (e.g. Roettgering et al. 1994; Blundell et al. 1998; De Breuck et al. 2004).

We find 29 sources in the ATHDFS with  $\alpha_{1.4\text{GHz}}^{2.5\text{GHz}} < -1.1$  (see Table 9). Most (21) of the sources have bright (I mag < 23) optical counterparts in ground based imaging. Another 4 sources are radio lobes of multiple component radio sources. The other 4 USS sources could be high redshift AGN. These candidates are listed in Table 12. Followup observations of these candidates are required to determine if these sources are HzRGs.

### 9. Summary

Deep radio observations of the Hubble Deep Field South region with  $1\sigma$  rms sensitivities of  $\sim 10 \mu\text{Jy}$  at 2.5, 5.2 and 8.7 GHz yield catalogues consisting of 71 sources at 2.5 GHz, 24 sources at 5.2 GHz and 6 sources at 8.7 GHz. We have constructed a consolidated radio catalogue from the four frequency observations of the ATHDFS, which has 473 individual radio sources.

Radio spectral indices were calculated for sources detected at more than one frequency. In deriving the spectral indices, care was taken to correct for spatial resolution effects. For sources detected at both 1.4 GHz and 2.5 GHz, we find the peak in the distribution of the spectral index  $\alpha_{1.4\text{GHz}}^{2.5\text{GHz}}$  is  $-0.5$ . We use the spectral index to identify possible AGN. Of the 136 sources with radio spectral information, 34 have flat or inverted spectra and are therefore classified as AGN.

We also identify some interesting radio sources in the ATHDFS survey. One source, ATHDFS\_223319.1-604428, is a radio galaxy at  $z = 0.65$  with a broad MgII emission line, and a possible FRI morphology. In the 1.4 GHz image we have also found a giant radio galaxy, ATHDFS\_223432.9-601239, which has an extent of 0.8 Mpc from lobe to lobe. This giant radio galaxy is at a redshift of  $z = 0.121$  and its spectrum is consistent with an old

stellar population. Three radio sources have radio SEDs which peak between 2 – 4 GHz, and hence are classed as Gigahertz Peaked Spectrum sources. Two of these GPS sources are not detected in HST flanking field observations to I (F814W) mag = 26.0, which implies they are either unusually underluminous in the optical or lie at high redshifts  $z \geq 2$ . Using the ultra-steep spectrum selection technique, we find there are 4 possible high redshift radio galaxies in our sample.

The HDFs has been the target of deep multicolor optical photometry and spectroscopy. The Spitzer Space Telescope has also imaged the HDFs in the infrared. The ATHDFS observations were carried out over several years, and hence it is also a good dataset to investigate time varying radio sources at these frequencies. Future papers in this series will present the optical/infrared identifications of the ATHDFS radio sources and an analysis of time variability.

MTH would like to acknowledge support from an Australian National University PhD Stipend Scholarship. The Australia Telescope Compact Array is part of the Australia Telescope, which is funded by the Commonwealth of Australia for operation as a National Facility managed by the CSIRO.

## REFERENCES

- Baum, S. A., Zirbel, E. L., & O’Dea, C. P. 1995, *ApJ*, 451, 88
- Bertin, E., & Arnouts, S. 1996, *A&AS*, 117, 393
- Bicknell, G. V., Dopita, M. A., & O’Dea, C. P. O. 1997, *ApJ*, 485, 112
- Blanton, M. R., et al. 2001, *AJ*, 121, 2358
- Blundell, K. M., & Rawlings, S. 2001, *ApJ*, 562, L5
- Blundell, K. M., Rawlings, S., Eales, S. A., Taylor, G. B., & Bradley, A. D. 1998, *MNRAS*, 295, 265
- Bock, D. C.-J., Large, M. I., & Sadler, E. M. 1999, *AJ*, 117, 1578
- Bondi, M., et al. 2003, *A&A*, 403, 857
- Cao, X., & Rawlings, S. 2004, *MNRAS*, 349, 1419
- Casertano, S., et al. 2000, *AJ*, 120, 2747



- Condon, J. J. 1984, ApJ, 287, 461
- Condon, J. J. 1989, ApJ, 338, 13
- Condon, J. J. 1992, ARA&A, 30, 575
- De Breuck, C., Hunstead, R. W., Sadler, E. M., Rocca-Volmerange, B., & Klamer, I. 2004, MNRAS, 347, 837
- De Breuck, C., van Breugel, W., Röttgering, H. J. A., & Miley, G. 2000, A&AS, 143, 303
- De Breuck, C., van Breugel, W., Stanford, S. A., Röttgering, H., Miley, G., & Stern, D. 2002, AJ, 123, 637
- Drake, C. L., McGregor, P. J., & Dopita, M. A. 2004, AJ, 128, 955
- Fanaroff, B. L., & Riley, J. M. 1974, MNRAS, 167, 31P
- Gardner, J. P., et al. 2000, AJ, 119, 486
- Hine, R. G., & Longair, M. S. 1979, MNRAS, 188, 111
- Hook, I. M., Shaver, P. A., Jackson, C. A., Wall, J. V., & Kellermann, K. I. 2003, A&A, 399, 469
- Huynh, M. T., Jackson, C. A., Norris, R. P., & Prandoni, I. 2005, AJ, 130, 1373
- Jackson, C. A., & Wall, J. V. 1999, MNRAS, 304, 160
- Kuncic, Z., Bicknell, G. V., & Dopita, M. A. 1998, ApJ, 495, L35
- Labbé, I., et al. 2003, AJ, 125, 1107
- Laing, R. A., Jenkins, C. R., Wall, J. V., & Unger, S. W. 1994, in The First Stromlo Symposium: The Physics of Active Galaxies. ASP Conference Series, Vol. 54, 1994, G.V. Bicknell, M.A. Dopita, and P.J. Quinn, Eds., p.201, 201
- Longair, M. S., & Lilly, S. J. 1984, Journal of Astrophysics and Astronomy, 5, 349
- Lucas, R. A., et al. 2003, AJ, 125, 398
- Marscher, A. P. 1988, ApJ, 334, 552
- Mauch, T., Murphy, T., Buttery, H. J., Curran, J., Hunstead, R. W., Piestrzynski, B., Robertson, J. G., & Sadler, E. M. 2003, MNRAS, 342, 1117

- Mutel, R. L., Hodges, M. W., & Phillips, R. B. 1985, *ApJ*, 290, 86
- Norris, R. P., et al. 2005, *AJ*, 130, 1358
- O’Dea, C. P. 1998, *PASP*, 110, 493
- O’Dea, C. P., Baum, S. A., & Stanghellini, C. 1991, *ApJ*, 380, 66
- Pence, W. 1976, *ApJ*, 203, 39
- Prandoni, I., Parma, P., Wieringa, M. H., de Ruiter, H. R., Gregorini, L., Mignano, A., Vettolani, G., & Ekers, R. D. 2006, *ArXiv Astrophysics e-prints*
- Reynolds, C. S., di Matteo, T., Fabian, A. C., Hwang, U., & Canizares, C. R. 1996, *MNRAS*, 283, L111
- Roettgering, H. J. A., Lacy, M., Miley, G. K., Chambers, K. C., & Saunders, R. 1994, *A&AS*, 108, 79
- Rowan-Robinson, M., Benn, C. R., Lawrence, A., McMahon, R. G., & Broadhurst, T. J. 1993, *MNRAS*, 263, 123
- Rudnick, G., et al. 2001, *AJ*, 122, 2205
- Sawicki, M., & Mallén-Ornelas, G. 2003, *AJ*, 126, 1208
- Teplitz, H. I., Hill, R. S., Malumuth, E. M., Collins, N. R., Gardner, J. P., Palunas, P., & Woodgate, B. E. 2001, *ApJ*, 548, 127
- Urry, C. M., & Padovani, P. 1995, *PASP*, 107, 803
- Urry, C. M., Scarpa, R., O’Dowd, M., Giavalisco, M., Falomo, R., Pesce, J. E., & Treves, A. 2002, *New Astronomy Review*, 46, 349
- Wall, J. V., Benn, C. R., Grueff, G., & Vigotti, M. 1986, *Highlights in Astronomy*, 7, 345
- Windhorst, R. A., Fomalont, E. B., Partridge, R. B., & Lowenthal, J. D. 1993, *ApJ*, 405, 498
- Windhorst, R. A., Miley, G. K., Owen, F. N., Kron, R. G., & Koo, D. C. 1985, *ApJ*, 289, 494
- Yahata, N., Lanzetta, K. M., Chen, H., Fernández-Soto, A., Pascarelle, S. M., Yahil, A., & Puetter, R. C. 2000, *ApJ*, 538, 493

### A. ATHDFS Combined Catalogue IDs

Table 13 contains the crossmatch data for the ATHDFS combined catalogue. This table is laid out as follows:

*Column (1)* — Source name.

*Column (2)* — Source ID in the 1.4 GHz catalogue.

*Column (3)* — Source ID in the 2.5 GHz catalogue. Low SNR sources from the supplementary catalogue are listed in brackets.

*Column (4)* — Source ID in the 5.2 GHz catalogue. Low SNR sources from the supplementary catalogue are listed in brackets.

*Column (5)* — Source ID in the 8.7 GHz catalogue. Low SNR sources from the supplementary catalogue are listed in brackets.

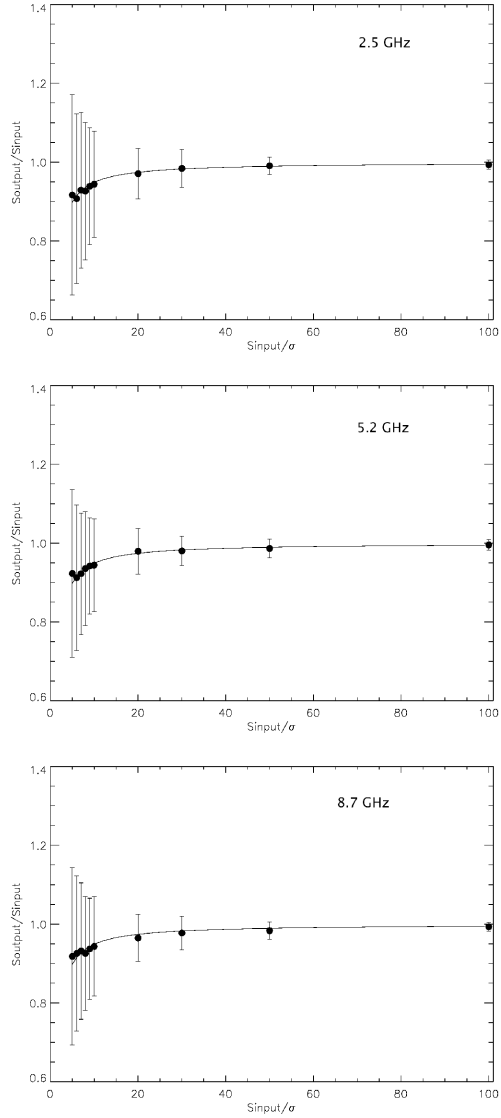


Fig. 1.— Source fluxes measured after the cleaning process ( $S_{\text{output}}$ ) normalised to the true source fluxes ( $S_{\text{input}}$ ), as a function of the input source signal-to-noise ( $S_{\text{input}}/\sigma_{\text{local}}$ ). Also shown are the best fit curves (see Section 3.1).

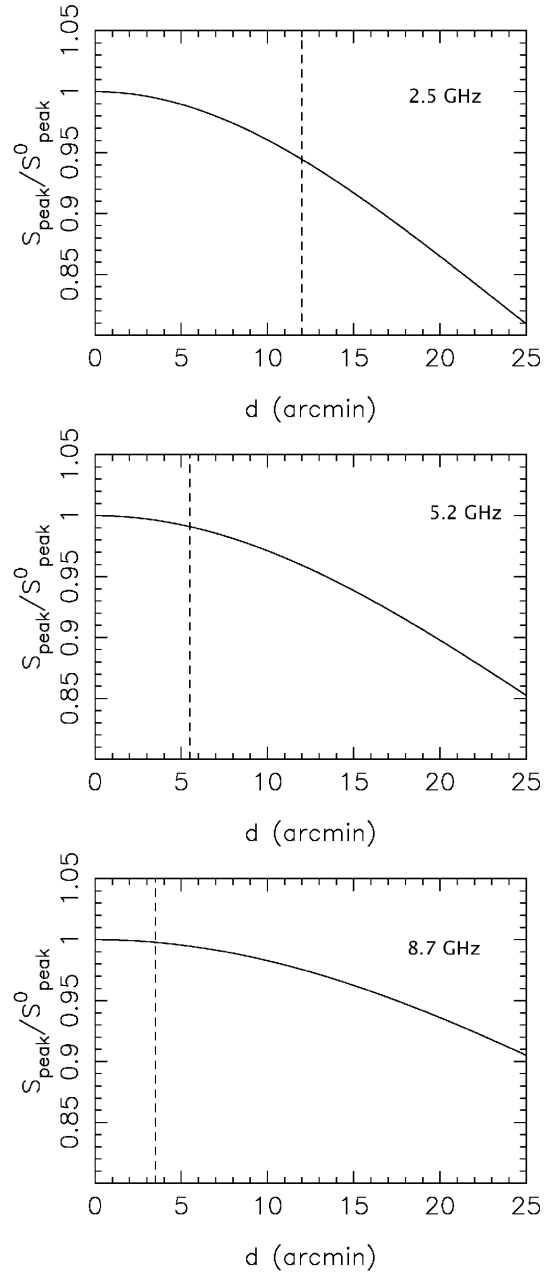


Fig. 2.— Bandwidth smearing effect, as a function of distance from the phase centre, for three ATHDFS images. The dashed lines indicate the maximum distance to which sources are catalogued for each image (see Section 3.2 for details).

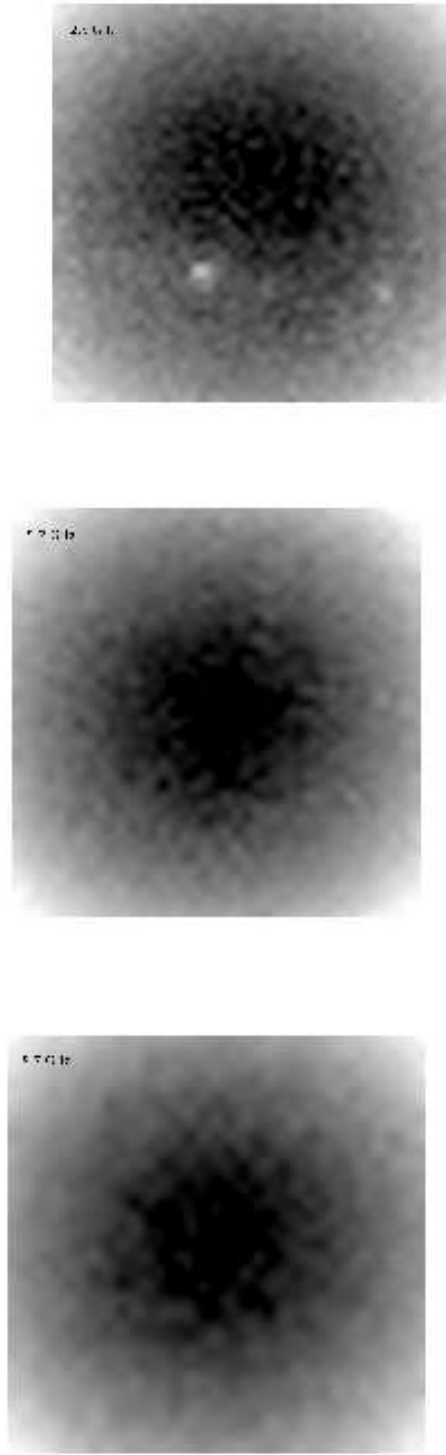


Fig. 3.— Grey scales of the noise maps obtained by SExtractor. The images are  $28 \times 28$  arcmin,  $12 \times 12$  arcmin, and  $8 \times 8$  arcmin, for 2.5, 5.2 and 8.7 GHz, respectively. The darker regions indicate lower noise.

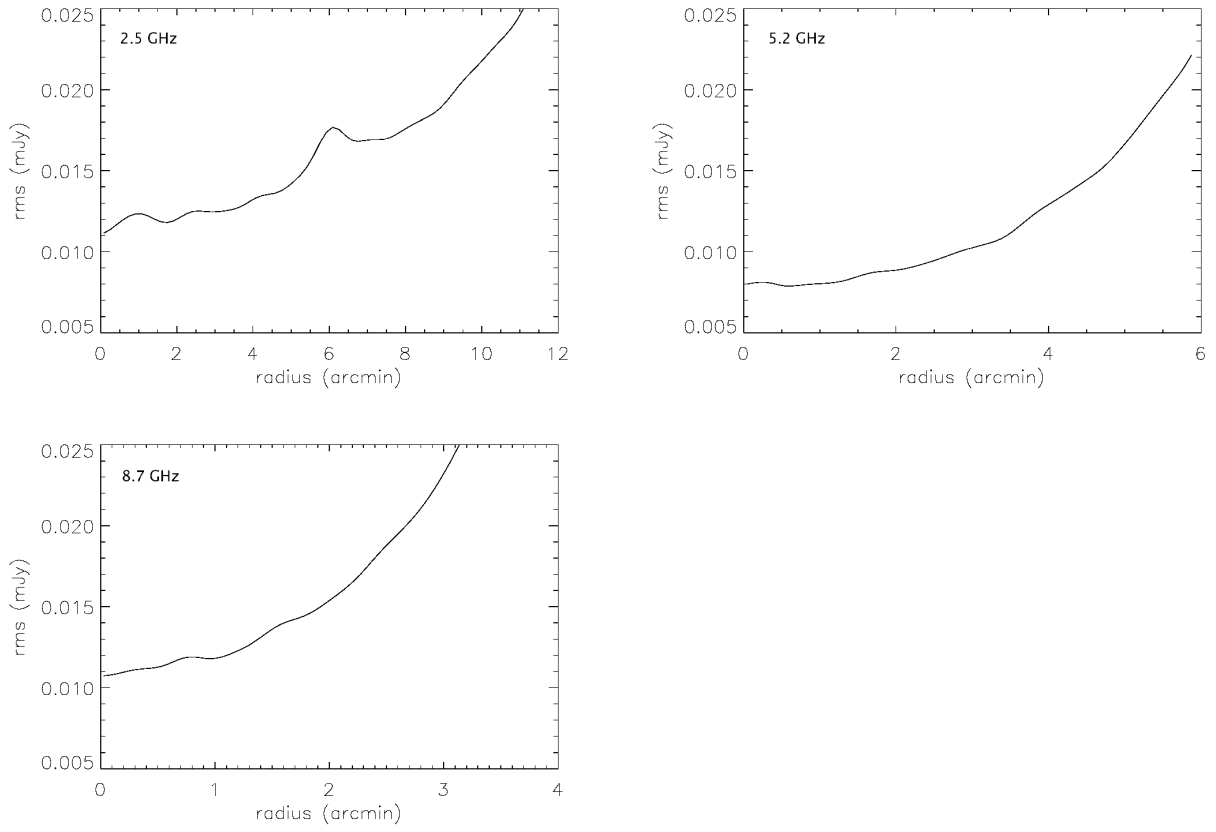


Fig. 4.— Noise (radially averaged) as a function of radial distance for the SExtractor noise maps of the ATHDFS images.

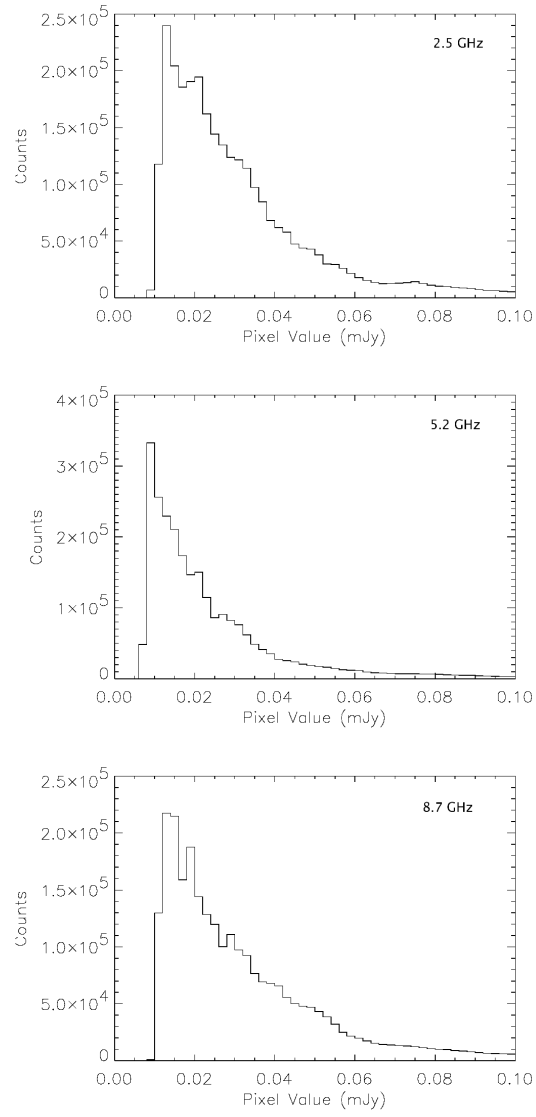


Fig. 5.— Distribution of the pixel values of the SEExtractor noise maps.



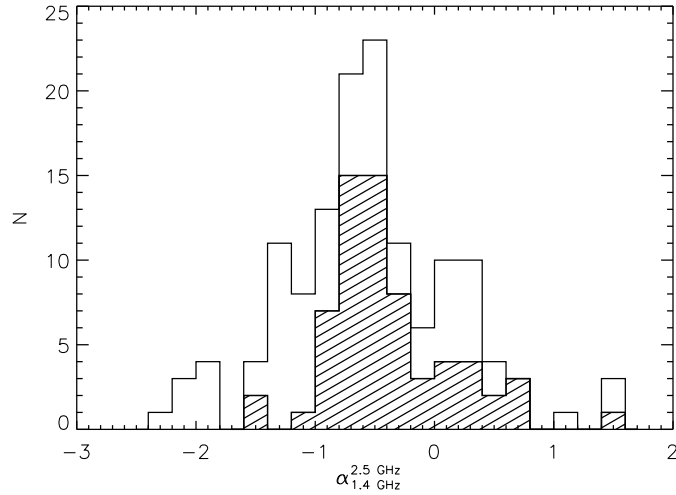


Fig. 6.— Distribution of the spectral index  $\alpha_{1.4\text{GHz}}^{2.5\text{GHz}}$  of the 136 sources detected at both 1.4 and 2.5 GHz. The hatched histogram shows sources with significant detections in each frequency, while the blank histogram includes the low signal to noise sources from the 2.5 GHz supplementary catalogue.

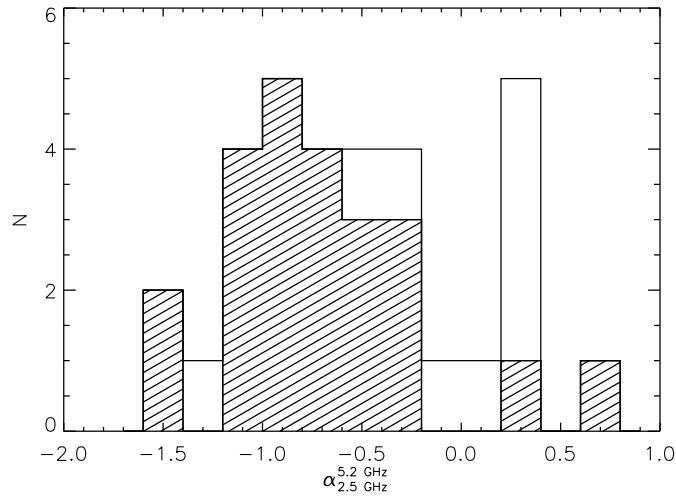


Fig. 7.— Distribution of the spectral index  $\alpha_{2.5\text{GHz}}^{5.2\text{GHz}}$  of the 32 sources detected at both 2.5 and 5.2 GHz. The hatched histogram shows sources with significant detections in each frequency, while the blank histogram includes the low signal to noise sources from the supplementary catalogues.

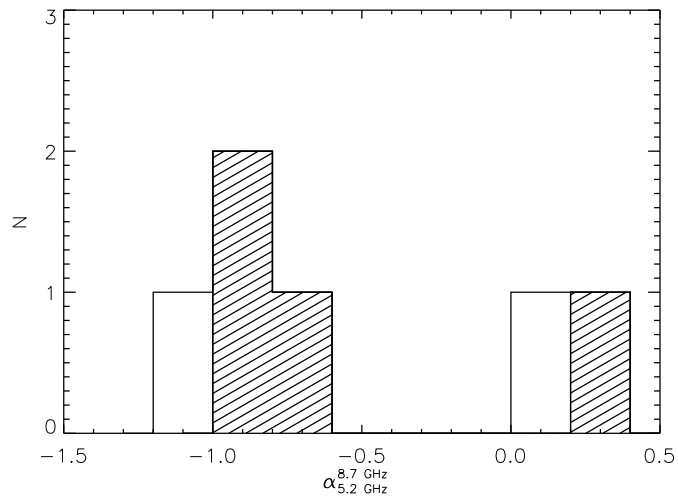


Fig. 8.— Distribution of the spectral index  $\alpha_{5.2\text{GHz}}^{8.7\text{GHz}}$  of the 6 sources detected at both 5.2 and 8.7 GHz. The hatched histogram shows sources with significant detections in each frequency, while the blank histogram includes the low signal to noise sources from the supplementary catalogues.

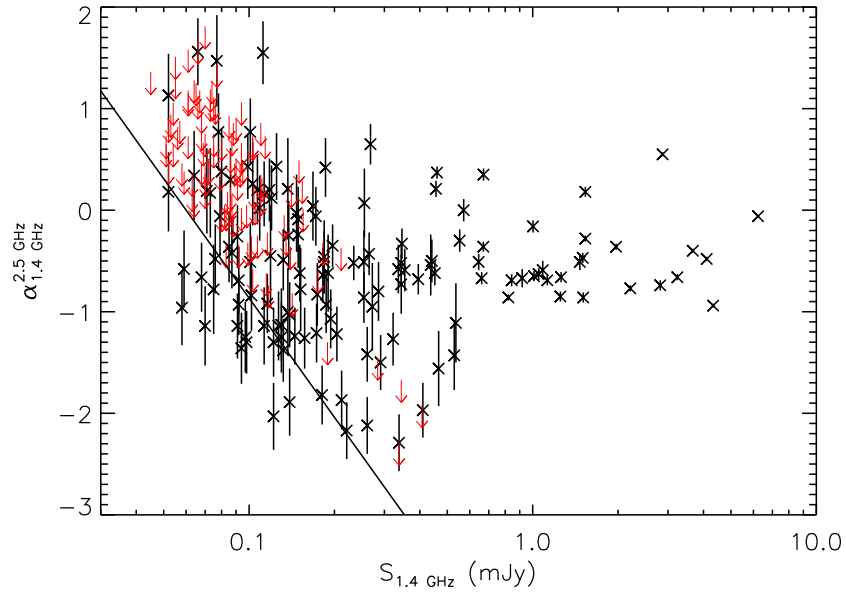


Fig. 9.— The spectral index  $\alpha_{1.4\text{GHz}}^{2.5\text{GHz}}$  vs 1.4 GHz flux density for the 1.4 GHz sources within the 2.5 GHz catalogued region. The red arrows mark upper limits of sources not detected at 2.5 GHz. The solid line shows the alpha upper limit assuming a detection limit of 0.06 mJy ( $5.5\sigma$ ) at 2.5 GHz.

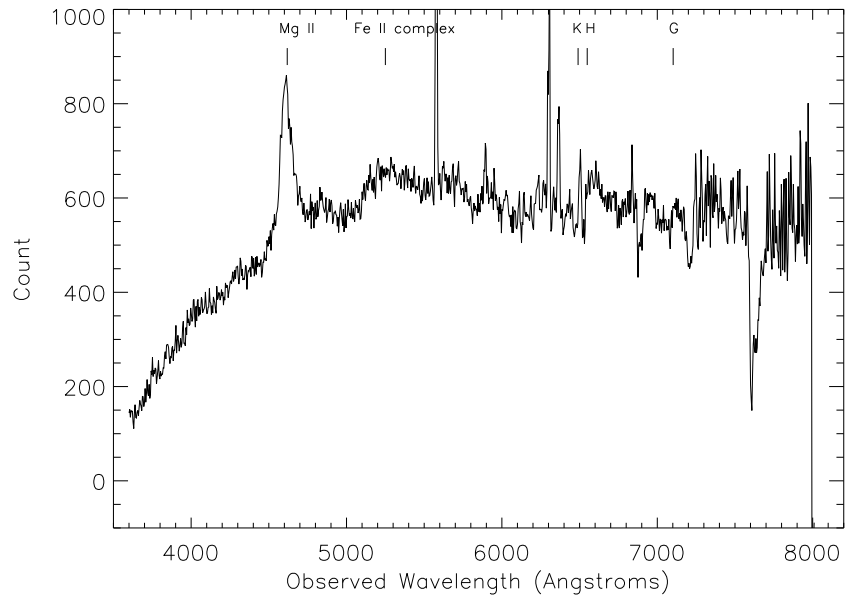


Fig. 10.— Low resolution 2dF optical spectrum of broadline emitting galaxy ATHDFS\_223319.1-604428. The MgII broadline emission and HK absorption features place this galaxy at  $z = 0.65$ . The strong features in the spectra at about 5600 and 6300 angstroms are artifacts from sky line subtraction.

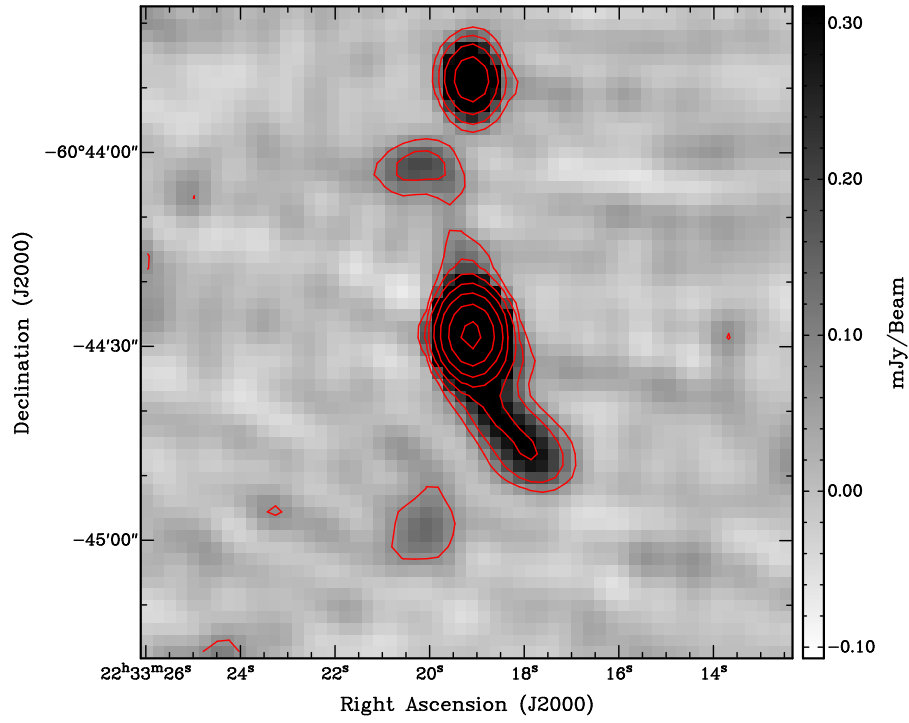


Fig. 11.— Grey scale 1.4 GHz image of ATHDFS\_223319.1-604428, overlaid with ATHDFS 1.4 GHz contours. The radio contour levels are set to  $3\sigma$ ,  $6\sigma$ ,  $12\sigma$ ,  $24\sigma$ ,  $48\sigma$ ,  $96$  and  $192\sigma$ .

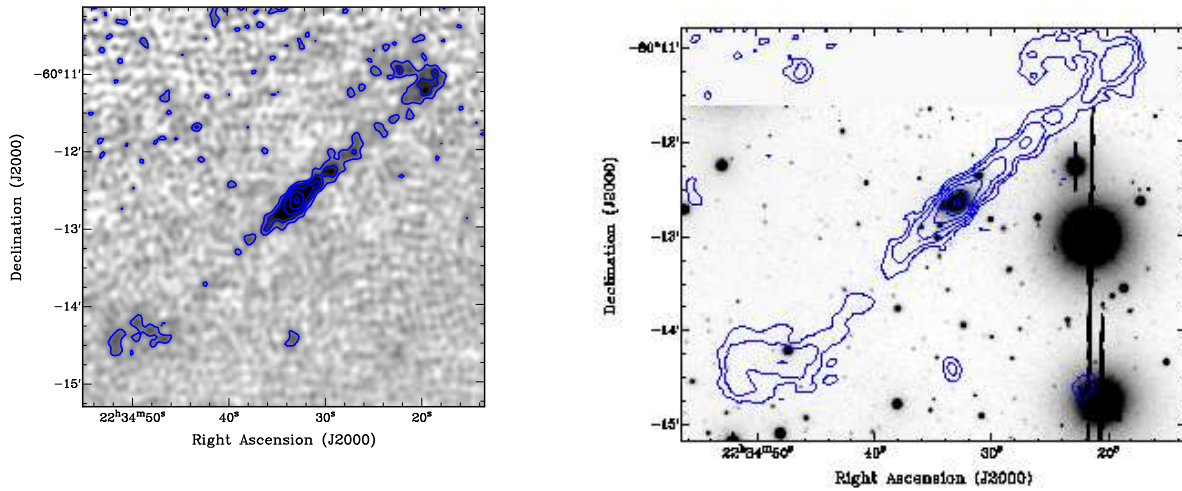


Fig. 12.— **Left:** Grey scale 1.4 GHz image of giant radio galaxy ATDFS\_223432.9-601239, overlaid with contours from the same image. The radio contour levels are set to  $3\sigma$ ,  $6\sigma$ ,  $12\sigma$ ,  $24\sigma$ , and  $48\sigma$ . **Right:** Contours from the tapered 1.4 GHz image on CTIO 4m Big Throughput Camera (BTC) I band optical image, showing the bright elliptical host galaxy. Low surface brightness regions of the lobe are more prominent in this tapered radio image. The radio contour levels are set to  $3\sigma$ ,  $6\sigma$ ,  $12\sigma$ ,  $24\sigma$ , and  $48\sigma$ .

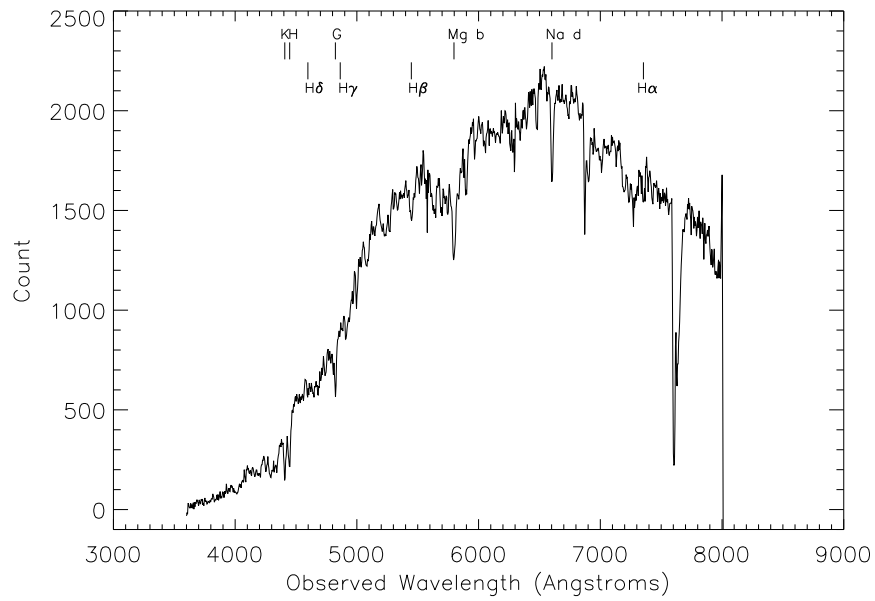


Fig. 13.— Low resolution 2dF optical spectrum of giant radio galaxy ATHDFS\_223432.9-601239. The H and K Ca II, G band, Mg and Na absorption features place this galaxy at  $z = 0.121$ . There is no significant H $\alpha$  or nebular line emission, and the higher order Balmer lines are in absorption. This implies that this galaxy has an old stellar population and there is no significant star formation taking place.

$\nu$ GHz	RA	Dec	Hours Observed	Synthesised Beam $b_{\text{maj}} \times b_{\text{min}}$	Beam PA	rms limit $\mu\text{Jy}$	$S_{\text{min}}$ $\mu\text{Jy}$
1.4	22 33 25.96	–60 38 09.0	345	7.1" $\times$ 6.2"	–5.5°	11.0	–168.5
2.5	22 33 25.96	–60 38 09.0	94	5.1" $\times$ 4.0"	1.7°	10.4	–486.7
5.2	22 32 56.22	–60 33 02.7	181	3.0" $\times$ 2.2"	10.7°	7.8	–42.3
8.7	22 32 56.22	–60 33 02.7	98	2.3" $\times$ 1.7"	–1.6°	11.0	–60.1

Table 1: Summary of the four frequency ATCA observations centred on the HDFs.

Image	$a$	$b$
2.5 GHz	$1.00 \pm 0.01$	$-0.51 \pm 0.54$
5.2 GHz	$1.00 \pm 0.01$	$-0.51 \pm 0.47$
8.7 GHz	$1.00 \pm 0.01$	$-0.53 \pm 0.49$

Table 2: Summary of clean bias fit parameters.



2.5 GHz			
SNR	sources in real image	sources in negative image	reliability (%)
>5.5	71	1	98.6
5 - 5.5	13	8	38.5
4 - 5	171	96	43.9
3 - 4	1300	1154	11.2
5.2 GHz			
SNR	sources in real image	sources in negative image	reliability (%)
> 5	24	1	96
4 - 5	56	35	37.5
3 - 4	818	828	~0
8.7 GHz			
SNR	sources in real image	sources in negative image	reliability (%)
> 5	6	0	100
4 - 5	30	33	~0
3 - 4	756	804	~0

Table 3: Summary of reliability estimates.

Table 4. 2.5 GHz catalogue.

ID	RA	$\sigma\alpha$	Dec	$\sigma\delta$	$S_{\text{peak}}$	$S_{\text{int}}$	$\theta_{\text{maj}}$	$\theta_{\text{min}}$	PA	$\text{SN}_{\text{local}}$	Flag
1	22:32:26.96	0.32	-60:47:46.0	0.46	0.194	0.292	3.99	2.27	-41.2	6.6	2
2	22:32:54.06	0.17	-60:47:37.0	0.34	0.222	0.228	...	...	...	8.2	2
3	22:33:33.27	0.28	-60:46:43.0	0.37	0.161	0.234	3.96	1.80	-47.4	7.8	2
4	22:33:29.95	0.37	-60:45:37.7	0.47	0.107	0.139	3.25	1.06	56.6	5.6	2
5	22:33:42.92	0.02	-60:45:24.8	0.04	1.409	1.588	2.08	1.18	11.8	65.8	
6	22:34:43.40	0.04	-60:44:52.9	0.06	1.388	1.673	2.45	1.60	-29.3	43.3	
7	22:32:10.36	0.01	-60:44:33.0	0.01	26.278	43.478	4.02	3.15	-50.4	481.6	
8	22:33:19.13	0.01	-60:44:28.3	0.01	5.222	5.969	2.23	1.24	4.0	205.5	
9	22:32:55.62	0.51	-60:44:00.4	0.28	0.117	0.191	...	...	...	7.0	2
10	22:33:19.14	0.05	-60:43:48.4	0.10	0.598	0.691	2.32	1.28	-9.8	29.0	
11	22:33:55.64	0.00	-60:43:15.7	0.00	99.193	111.800	1.79	1.44	-14.3	1202.0	
12	22:34:27.34	0.07	-60:42:58.8	0.13	0.550	0.596	2.03	0.50	-3.9	20.9	
13	22:33:12.65	0.28	-60:42:26.3	0.35	0.109	0.137	...	...	...	7.5	2
14	22:34:37.29	0.02	-60:42:14.3	0.02	3.261	3.876	2.23	1.54	-51.7	111.6	
15	22:33:38.93	0.26	-60:42:16.6	0.71	0.100	0.132	...	...	...	5.5	2
16	22:33:59.86	0.26	-60:41:55.4	0.41	0.132	0.162	2.63	1.60	37.4	6.8	2
17	22:32:24.53	0.01	-60:41:13.0	0.02	2.608	3.052	2.22	1.24	61.3	147.4	
18	22:34:48.31	0.46	-60:40:41.9	0.52	0.153	0.290	4.59	3.79	71.1	5.9	2
19	22:34:17.81	0.03	-60:40:09.4	0.05	0.977	1.092	1.72	1.22	66.8	52.0	
20	22:32:20.57	0.15	-60:39:31.1	0.32	0.136	0.129	...	...	...	8.3	2
21	22:32:45.65	0.05	-60:38:57.4	0.07	0.482	0.536	1.84	0.91	-60.4	35.4	
22	22:32:06.08	0.38	-60:38:57.2	0.41	0.134	0.222	4.99	1.85	-54.1	7.1	2
23	22:33:07.17	0.29	-60:38:46.4	0.47	0.064	0.074	1.93	1.55	18.2	5.7	2
24	22:33:35.94	0.26	-60:38:28.4	0.53	0.081	0.092	...	...	...	5.6	2
25	22:34:32.16	0.11	-60:38:15.0	0.18	0.288	0.371	2.88	1.97	-18.5	15.9	2

Table 4—Continued

ID	RA	$\sigma\alpha$	Dec	$\sigma\delta$	$S_{\text{peak}}$	$S_{\text{int}}$	$\theta_{\text{maj}}$	$\theta_{\text{min}}$	PA	$\text{SN}_{\text{local}}$	Flag
26	22:34:18.64	0.11	−60:38:08.3	0.17	0.218	0.244	1.92	1.13	−33.5	15.2	
27	22:34:42.67	0.40	−60:38:03.2	0.36	0.141	0.215	4.54	0.94	−66.9	6.9	2
28	22:34:36.95	0.09	−60:37:54.8	0.13	0.379	0.453	2.07	1.79	−77.4	20.4	
29	22:33:46.98	0.34	−60:37:53.5	0.41	0.062	0.076	2.56	1.06	−89.3	5.9	2
30	22:33:49.99	0.12	−60:37:41.0	0.17	0.232	0.421	5.13	2.94	−38.2	20.1	
31	22:33:50.71	0.44	−60:37:45.3	0.49	0.069	0.122	4.33	3.35	71.6	6.0	
32	22:32:32.83	0.07	−60:37:37.3	0.11	0.373	0.489	3.23	1.79	27.5	26.9	
33	22:34:04.83	0.03	−60:37:32.5	0.03	1.403	2.158	4.20	1.73	−83.7	96.3	
34	22:32:36.60	0.18	−60:36:57.7	0.44	0.095	0.111	...	...	...	7.5	2
35	22:34:00.30	0.02	−60:36:53.3	0.04	0.979	1.399	3.94	2.11	7.6	75.6	
36	22:34:04.36	0.04	−60:36:38.7	0.06	0.638	0.743	2.26	1.47	−0.9	44.3	
37	22:34:29.97	0.04	−60:36:29.6	0.07	0.698	0.785	2.19	0.64	43.6	37.9	
38	22:33:16.58	0.05	−60:36:27.5	0.07	0.376	0.451	2.45	1.03	88.7	36.1	
39	22:32:32.45	0.26	−60:35:42.3	0.61	0.138	0.334	7.83	3.39	−10.1	7.9	
40	22:32:32.60	0.40	−60:35:53.5	0.80	0.098	0.236	7.11	3.97	−5.3	5.5	
41	22:32:24.02	0.04	−60:35:37.8	0.07	0.620	0.836	3.48	1.89	−18.6	42.1	
42	22:33:38.82	0.16	−60:35:24.1	0.17	0.145	0.159	...	...	...	12.6	
43	22:32:08.36	0.09	−60:35:19.0	0.12	0.461	0.551	2.39	1.31	60.8	21.6	
44	22:33:45.01	0.19	−60:35:15.9	0.22	0.144	0.211	3.46	2.39	−79.7	12.0	
45	22:34:10.15	0.20	−60:35:10.2	0.39	0.087	0.081	...	...	...	6.6	2
46	22:33:50.53	0.03	−60:35:03.9	0.05	0.678	0.724	1.49	0.24	77.0	49.4	
47	22:32:30.25	0.22	−60:35:03.5	0.36	0.112	0.128	2.26	0.97	35.3	7.4	2
48	22:34:38.61	0.02	−60:34:50.4	0.02	2.128	2.776	2.98	1.82	50.1	113.1	
49	22:32:45.53	0.14	−60:34:19.1	0.20	0.150	0.161	...	...	...	11.8	
50	22:33:27.67	0.05	−60:34:14.3	0.07	0.466	0.498	1.38	0.75	−69.7	34.1	

Table 4—Continued

ID	RA	$\sigma\alpha$	Dec	$\sigma\delta$	$S_{\text{peak}}$	$S_{\text{int}}$	$\theta_{\text{maj}}$	$\theta_{\text{min}}$	PA	$\text{SN}_{\text{local}}$	Flag
51	22:33:06.06	0.12	−60:33:50.3	0.17	0.203	0.288	2.92	2.85	−15.1	17.5	
52	22:33:29.82	0.27	−60:33:51.3	0.39	0.081	0.091	...	...	...	6.6	2
53	22:32:58.61	0.03	−60:33:46.6	0.05	0.617	0.658	1.48	0.47	−58.5	48.1	
54	22:34:20.96	0.01	−60:33:36.6	0.02	2.088	2.453	1.93	1.74	77.3	130.4	
55	22:33:37.58	0.04	−60:33:29.1	0.07	0.622	0.718	2.44	1.14	7.7	42.8	
56	22:33:27.96	0.14	−60:33:04.6	0.23	0.151	0.187	2.71	1.75	21.9	12.5	
57	22:33:08.56	0.10	−60:32:51.2	0.16	0.264	0.394	4.64	1.46	−33.6	20.6	
58	22:33:09.00	0.26	−60:32:56.2	0.51	0.078	0.101	3.33	1.61	6.0	6.1	
59	22:33:23.25	0.04	−60:32:49.2	0.06	0.524	0.561	1.37	0.73	84.4	44.8	
60	22:32:12.94	0.08	−60:32:34.6	0.07	0.851	1.574	6.09	1.52	−56.3	41.2	
61	22:32:12.95	0.10	−60:32:42.8	0.18	0.458	0.903	5.87	3.23	16.2	22.2	
62	22:32:29.57	0.20	−60:32:42.9	0.25	0.140	0.143	...	...	...	8.8	2
63	22:33:31.62	0.18	−60:32:22.2	0.16	0.203	0.286	3.89	0.61	81.3	14.5	
64	22:33:51.15	0.33	−60:31:53.1	0.27	0.079	0.071	...	...	...	5.9	2
65	22:34:04.00	0.31	−60:30:37.7	0.45	0.100	0.122	2.55	1.50	−50.8	6.0	2
66	22:32:36.56	0.05	−60:30:00.4	0.07	0.766	0.877	2.37	0.50	−48.0	36.7	
67	22:34:30.07	0.19	−60:29:58.7	0.24	0.243	0.280	2.21	0.60	−82.3	9.8	2
68	22:33:55.55	0.03	−60:29:56.4	0.04	1.106	1.247	2.07	1.17	18.2	62.7	
69	22:33:16.81	0.04	−60:29:34.5	0.07	0.699	0.811	2.61	1.00	15.9	39.6	
70	22:33:07.14	0.15	−60:28:27.5	0.24	0.192	0.214	...	...	...	11.0	
71	22:32:55.84	0.42	−60:28:09.6	0.51	0.133	0.244	4.24	3.85	72.1	6.0	2



Table 5. 5.2 GHz catalogue.

ID	RA	$\sigma\alpha$	Dec	$\sigma\delta$	$S_{\text{peak}}$	$S_{\text{int}}$	$\theta_{\text{maj}}$	$\theta_{\text{min}}$	PA	$\text{SN}_{\text{local}}$	Flag
1	22:32:32.84	0.08	-60:37:37.1	0.19	0.216	0.280	...	...	...	11.2	
2	22:33:16.56	0.11	-60:36:27.4	0.18	0.141	0.204	2.12	1.22	-35.9	9.7	
3	22:32:32.70	0.19	-60:35:54.9	0.32	0.089	0.141	2.76	1.24	31.1	6.2	
4	22:32:32.26	0.20	-60:35:41.4	0.39	0.076	0.115	2.79	1.05	24.7	5.4	
5	22:32:24.04	0.04	-60:35:37.8	0.11	0.295	0.396	2.56	0.32	-7.5	18.7	
6	22:32:30.21	0.13	-60:35:03.5	0.29	0.076	0.083	...	...	...	5.9	2
7	22:32:43.32	0.23	-60:34:42.5	0.30	0.047	0.053	...	...	...	5.1	2
8	22:32:45.51	0.13	-60:34:19.0	0.16	0.060	0.049	...	...	...	6.9	2
9	22:33:27.66	0.04	-60:34:14.2	0.08	0.262	0.269	...	...	...	21.0	
10	22:33:29.74	0.19	-60:33:51.9	0.26	0.073	0.082	...	...	...	5.3	2
11	22:32:43.49	0.13	-60:33:51.5	0.18	0.066	0.073	...	...	...	7.7	2
12	22:33:06.05	0.15	-60:33:50.2	0.26	0.066	0.123	2.96	1.84	-23.7	8.0	2
13	22:32:58.59	0.02	-60:33:46.6	0.03	0.404	0.394	...	...	...	46.9	
14	22:33:37.58	0.05	-60:33:29.3	0.10	0.324	0.373	1.40	0.66	5.4	17.5	
15	22:33:27.98	0.17	-60:33:04.5	0.22	0.093	0.114	...	...	...	7.2	2
16	22:33:08.61	0.06	-60:32:51.6	0.14	0.139	0.196	2.66	0.32	-20.6	15.3	2
17	22:33:23.25	0.03	-60:32:49.2	0.04	0.360	0.370	...	...	...	32.9	
18	22:32:12.91	0.23	-60:32:43.9	0.53	0.148	0.657	6.65	3.39	-1.6	6.3	2
19	22:32:29.55	0.07	-60:32:43.6	0.16	0.108	0.117	...	...	...	10.5	
20	22:32:13.07	0.10	-60:32:35.5	0.15	0.338	0.716	3.48	1.89	-35.3	14.5	
21	22:33:31.60	0.10	-60:32:22.2	0.20	0.120	0.130	...	...	...	8.5	2
22	22:32:36.57	0.03	-60:30:00.4	0.04	0.394	0.446	...	...	...	32.9	
23	22:33:16.80	0.02	-60:29:34.7	0.05	0.502	0.569	1.45	0.44	1.5	37.4	
24	22:33:07.20	0.37	-60:28:27.5	0.25	0.101	0.186	...	...	...	6.2	2



Table 6. 8.7 GHz catalogue.

ID	RA	$\sigma\alpha$	Dec	$\sigma\delta$	$S_{\text{peak}}$	$S_{\text{int}}$	$\theta_{\text{maj}}$	$\theta_{\text{min}}$	PA	$\text{SN}_{\text{local}}$	Flag
1	22:32:43.47	0.06	-60:33:51.0	0.20	0.114	0.103	...	...	...	8.0	2
2	22:32:58.59	0.03	-60:33:46.6	0.07	0.238	0.260	...	...	...	19.4	
3	22:33:06.26	0.09	-60:33:07.9	0.35	0.071	0.092	...	...	...	5.6	2
4	22:32:42.66	0.06	-60:32:58.1	0.20	0.077	0.044	...	...	...	5.3	2
5	22:33:08.61	0.08	-60:32:52.3	0.19	0.092	0.074	...	...	...	6.2	2
6	22:33:23.24	0.04	-60:32:48.9	0.17	0.223	0.181	...	...	...	7.9	2



Table 7. 2.5 GHz supplementary catalogue. These are low SNR ( $3 - 5.5\sigma$ ) sources with a priori 1.4 GHz positions.  
The ID numbering starts from the end of the main catalogue.

ID	RA	$\sigma\alpha$	Dec	$\sigma\delta$	$S_{\text{peak}}$	$S_{\text{int}}$	$\theta_{\text{maj}}$	$\theta_{\text{min}}$	PA	SN <sub>local</sub>	Flag
72	22:34:00.44	0.33	-60:49:03.2	0.63	0.117	0.096	...	...	...	3.8	2
73	22:34:07.63	0.57	-60:48:47.8	0.57	0.085	0.073	...	...	...	3.0	2
74	22:33:37.76	0.59	-60:48:33.1	0.85	0.091	0.113	...	...	...	3.6	2
75	22:32:55.85	0.48	-60:48:22.8	0.81	0.103	0.178	4.69	3.12	15.6	4.3	2
76	22:33:59.72	0.68	-60:48:04.6	0.67	0.092	0.092	...	...	...	3.4	2
77	22:32:43.13	0.43	-60:47:58.6	0.69	0.103	0.107	...	...	...	4.0	2
78	22:34:14.73	0.24	-60:47:54.2	0.67	0.140	0.135	...	...	...	4.4	2
79	22:33:30.51	0.35	-60:46:23.5	0.66	0.096	0.125	3.59	1.25	-23.5	4.7	2
80	22:34:34.59	0.62	-60:46:03.2	0.62	0.127	0.179	3.67	1.39	83.0	3.9	2
81	22:34:08.14	0.67	-60:45:35.2	0.91	0.060	0.071	...	...	...	3.0	2
82	22:33:11.43	0.60	-60:44:51.7	1.22	0.059	0.091	4.68	2.16	-12.6	3.0	2
83	22:32:43.93	0.77	-60:44:39.0	1.01	0.075	0.239	8.22	5.25	-33.7	4.2	2
84	22:34:39.07	0.97	-60:44:36.6	0.41	0.110	0.147	...	...	...	3.6	2
85	22:34:22.46	0.87	-60:44:12.4	0.38	0.078	0.073	...	...	...	3.1	2
86	22:32:40.26	0.28	-60:43:06.1	0.31	0.098	0.075	...	...	...	5.3	2
87	22:34:25.89	0.49	-60:42:32.1	0.38	0.129	0.113	...	...	...	4.8	2
88	22:32:55.33	0.43	-60:41:51.8	0.92	0.046	0.046	...	...	...	3.1	2
89	22:33:39.44	0.77	-60:41:31.4	0.56	0.048	0.046	...	...	...	3.1	2
90	22:33:48.47	0.91	-60:40:27.9	0.57	0.047	0.062	...	...	...	3.7	2
91	22:34:29.80	0.80	-60:40:19.3	0.47	0.080	0.159	6.28	1.75	88.5	4.7	2
92	22:34:38.05	0.50	-60:39:51.8	0.43	0.074	0.058	...	...	...	3.5	2
93	22:33:24.65	0.32	-60:39:34.6	0.50	0.059	0.056	...	...	...	4.7	2
94	22:32:07.79	0.87	-60:39:27.9	1.09	0.076	0.205	7.21	4.54	38.9	3.6	2
95	22:32:58.92	0.96	-60:39:04.0	0.53	0.033	0.036	...	...	...	3.1	2
96	22:34:57.38	0.30	-60:38:42.1	0.60	0.128	0.149	...	...	...	5.0	2

Table 7—Continued

ID	RA	$\sigma_\alpha$	Dec	$\sigma_\delta$	$S_{\text{peak}}$	$S_{\text{int}}$	$\theta_{\text{maj}}$	$\theta_{\text{min}}$	PA	$\text{SN}_{\text{local}}$	Flag
97	22:34:50.34	0.96	-60:38:44.7	0.61	0.070	0.085	...	...	...	3.0	
98	22:32:32.41	0.32	-60:38:43.3	0.64	0.076	0.065	...	...	...	4.8	2
99	22:32:48.35	0.59	-60:38:06.5	0.75	0.045	0.060	2.84	2.03	84.5	3.5	2
100	22:34:41.58	0.40	-60:37:40.6	0.54	0.079	0.079	...	...	...	4.1	2
101	22:34:37.70	0.34	-60:37:27.2	0.78	0.090	0.109	...	...	...	4.5	2
102	22:34:17.25	0.28	-60:37:25.2	0.45	0.081	0.079	...	...	...	5.2	2
103	22:33:41.24	0.29	-60:37:25.3	1.09	0.054	0.089	6.64	0.24	0.8	4.3	2
104	22:32:02.49	0.32	-60:37:14.2	0.52	0.099	0.103	1.23	0.39	-56.9	4.8	2
105	22:33:43.85	0.32	-60:36:50.6	0.87	0.040	0.035	...	...	...	3.3	2
106	22:34:06.81	0.65	-60:36:38.8	0.70	0.040	0.039	...	...	...	3.0	2
107	22:31:58.23	0.56	-60:36:35.1	1.08	0.078	0.109	...	...	...	3.4	2
108	22:34:51.98	0.34	-60:36:31.7	0.61	0.127	0.194	4.54	2.08	23.9	5.4	2
109	22:33:41.92	0.54	-60:36:32.1	0.73	0.062	0.098	5.42	0.64	42.1	4.6	2
110	22:34:56.23	0.73	-60:36:17.8	0.76	0.089	0.121	...	...	...	3.4	2
111	22:32:29.84	0.39	-60:35:43.8	0.47	0.060	0.053	...	...	...	4.0	2
112	22:32:52.95	0.60	-60:35:39.8	1.14	0.041	0.066	4.74	2.42	17.0	3.1	2
113	22:34:35.48	0.41	-60:35:32.2	0.46	0.096	0.103	...	...	...	4.8	2
114	22:32:29.30	0.38	-60:34:59.5	0.70	0.077	0.110	4.33	1.64	23.3	4.8	2
115	22:34:31.75	0.78	-60:34:56.4	0.92	0.057	0.098	4.27	3.16	58.6	3.2	2
116	22:34:25.05	0.78	-60:34:53.0	0.92	0.058	0.101	4.45	3.12	56.3	3.3	2
117	22:34:01.04	0.43	-60:34:25.1	0.56	0.043	0.037	...	...	...	3.5	2
118	22:31:53.16	0.38	-60:34:23.5	0.54	0.079	0.053	...	...	...	3.1	2
119	22:33:12.02	0.64	-60:34:17.6	0.50	0.044	0.039	...	...	...	3.6	2
120	22:34:34.07	0.76	-60:34:08.7	0.55	0.080	0.139	5.18	1.68	86.5	4.2	2
121	22:32:43.46	0.19	-60:33:51.5	0.73	0.054	0.032	...	...	...	3.6	2

Table 7—Continued

ID	RA	$\sigma_\alpha$	Dec	$\sigma_\delta$	$S_{\text{peak}}$	$S_{\text{int}}$	$\theta_{\text{maj}}$	$\theta_{\text{min}}$	PA	$\text{SN}_{\text{local}}$	Flag
122	22:32:53.22	0.42	-60:33:28.7	0.39	0.054	0.047	...	...	...	4.3	2
123	22:33:03.30	0.43	-60:31:34.5	0.71	0.055	0.059	...	...	...	3.7	2
124	22:32:54.39	0.33	-60:31:31.8	0.37	0.059	0.043	...	...	...	4.3	2
125	22:33:51.87	0.61	-60:31:16.9	1.01	0.039	0.047	...	...	...	3.0	2
126	22:33:45.07	0.26	-60:30:39.0	0.74	0.060	0.054	...	...	...	3.9	2
127	22:34:05.18	0.43	-60:30:28.6	0.92	0.070	0.097	...	...	...	4.1	2
128	22:32:41.43	0.34	-60:30:24.5	0.57	0.063	0.040	...	...	...	3.5	2
129	22:32:16.62	0.24	-60:30:17.9	0.49	0.111	0.093	...	...	...	4.9	2
130	22:33:29.14	0.47	-60:29:32.6	0.67	0.081	0.122	3.89	2.44	39.9	4.5	2
131	22:33:01.98	0.52	-60:29:27.5	1.32	0.049	0.058	...	...	...	3.0	2
132	22:34:15.40	0.60	-60:29:24.7	0.58	0.098	0.128	...	...	...	4.4	2
133	22:34:07.54	0.69	-60:29:12.3	1.08	0.078	0.123	...	...	...	3.7	2
134	22:34:20.20	0.53	-60:28:59.9	0.38	0.116	0.147	...	...	...	5.2	2
135	22:33:07.71	0.73	-60:28:55.8	0.66	0.048	0.044	...	...	...	3.0	2
136	22:33:26.99	0.51	-60:28:50.7	0.60	0.093	0.143	4.68	1.39	-51.3	4.9	2
137	22:32:40.80	0.63	-60:27:55.9	0.72	0.069	0.069	...	...	...	3.0	2
138	22:33:11.58	1.08	-60:27:22.8	1.06	0.075	0.161	6.88	2.46	-53.6	3.1	2
139	22:33:17.23	1.46	-60:27:14.6	0.40	0.060	0.072	...	...	...	3.0	2
140	22:33:42.28	0.28	-60:26:37.5	0.48	0.090	0.050	...	...	...	3.4	2
141	22:33:35.16	0.45	-60:26:15.6	0.58	0.123	0.201	3.71	3.37	-63.0	5.2	2
142	22:33:22.42	0.41	-60:26:08.5	0.61	0.083	0.043	...	...	...	3.1	2



ID	Ra	$\sigma\alpha$	Dec	$\sigma\delta$	$S_{\text{peak}}$	$S_{\text{int}}$	$\theta_{\text{maj}}$	$\theta_{\text{min}}$	PA	$\text{SN}_{\text{local}}$	Flag
5.2 GHz											
25	22:32:53.08	0.85	-60:35:39.1	0.85	0.036	0.035	...	...	...	3.7	2
26	22:32:29.22	0.30	-60:34:59.9	0.43	0.054	0.080	2.49	1.02	45.0	4.2	2
27	22:32:31.67	0.28	-60:34:24.3	0.58	0.039	0.059	2.49	1.23	-15.4	3.5	2
28	22:33:12.04	0.35	-60:34:17.2	0.51	0.029	0.036	...	...	...	3.3	2
29	22:32:47.65	0.22	-60:33:36.0	0.34	0.038	0.045	...	...	...	4.4	2
30	22:33:17.73	0.29	-60:32:35.1	0.37	0.037	0.039	...	...	...	3.7	2
31	22:33:03.29	0.32	-60:31:34.1	0.36	0.035	0.040	...	...	...	4.0	2
32	22:32:54.29	0.79	-60:31:31.0	0.79	0.035	0.034	...	...	...	3.9	2
33	22:33:16.17	0.06	-60:31:27.8	0.39	0.040	0.024	...	...	...	4.2	2
34	22:32:56.48	0.29	-60:30:57.4	0.45	0.030	0.034	...	...	...	3.4	2
35	22:33:04.89	0.27	-60:30:30.9	0.39	0.033	0.030	...	...	...	3.2	2
36	22:32:41.45	0.81	-60:30:25.7	0.81	0.038	0.037	...	...	...	3.8	2
37	22:33:04.08	0.33	-60:30:12.8	0.59	0.035	0.045	...	...	...	3.2	2
38	22:32:53.74	0.14	-60:29:46.4	0.37	0.040	0.029	...	...	...	3.9	2
39	22:33:29.24	0.61	-60:29:33.8	0.36	0.068	0.107	...	...	...	3.2	2
40	22:33:01.77	0.38	-60:29:32.1	0.66	0.035	0.055	2.53	1.41	25.4	3.0	2
41	22:32:36.22	0.10	-60:28:54.5	0.27	0.053	0.024	...	...	...	3.4	2
42	22:32:55.95	0.26	-60:28:10.2	0.26	0.076	0.086	...	...	...	4.7	2
8.7 GHz											
7	22:32:45.56	0.08	-60:34:19.6	0.21	0.075	0.052	...	...	...	4.7	2
8	22:33:06.21	0.21	-60:33:50.2	0.28	0.042	0.035	...	...	...	3.1	2

Table 8: 5.2 and 8.7 GHz supplementary catalogues. These are low SNR ( $3 - 5\sigma$ ) sources with a priori 1.4 GHz positions. The ID numbering starts from the end of the main catalogue.

Table 9. The combined ATHDFS catalogue. Flux densities for sources from the supplementary catalogues are listed in brackets. The spectral indices are calculated from flux densities measured on low resolution images, as described in Section 7.

source name	RA	Dec	Coord Flag	$S_{1.4\text{GHz}}$	$S_{2.5\text{GHz}}$	$S_{5.2\text{GHz}}$	$S_{8.7\text{GHz}}$	$\alpha_{1.4\text{GHz}}^{2.5\text{GHz}}$	$\alpha_{2.5\text{GHz}}^{5.2\text{GHz}}$	$\alpha_{5.2\text{GHz}}^{8.7\text{GHz}}$	AGN flag
ATHDFS_J223303.6-605751	22:33:03.62	-60:57:51.6	L	0.508	-	-	-	-	-	-	
ATHDFS_J223325.8-605729	22:33:25.88	-60:57:29.3	L	0.162	-	-	-	-	-	-	
ATHDFS_J223255.6-605656	22:32:55.62	-60:56:56.5	L	0.375	-	-	-	-	-	-	
ATHDFS_J223246.3-605654	22:32:46.30	-60:56:54.0	L	0.254	-	-	-	-	-	-	
ATHDFS_J223403.4-605640	22:34:03.43	-60:56:40.3	L	0.210	-	-	-	-	-	-	
ATHDFS_J223243.8-605608A	22:32:43.80	-60:56:08.8	L	0.363	-	-	-	-	-	-	
ATHDFS_J223243.8-605608B	22:32:44.89	-60:56:03.7	L	0.176	-	-	-	-	-	-	
ATHDFS_J223410.5-605545A	22:34:10.58	-60:55:45.4	L	2.106	-	-	-	-	-	-	
ATHDFS_J223410.5-605545B	22:34:09.50	-60:55:59.6	L	2.443	-	-	-	-	-	-	
ATHDFS_J223308.5-605544	22:33:08.50	-60:55:44.3	L	3.643	-	-	-	-	-	-	
ATHDFS_J223314.6-605543	22:33:14.63	-60:55:43.5	L	0.322	-	-	-	-	-	-	
ATHDFS_J223316.9-605533	22:33:16.98	-60:55:33.6	L	0.420	-	-	-	-	-	-	
ATHDFS_J223353.9-605452	22:33:53.92	-60:54:52.1	L	5.918	-	-	-	-	-	-	
ATHDFS_J223334.6-605455	22:33:34.67	-60:54:55.9	L	0.451	-	-	-	-	-	-	
ATHDFS_J223214.8-605430	22:32:14.85	-60:54:30.2	L	18.601	-	-	-	-	-	-	
ATHDFS_J223448.4-605417	22:34:48.45	-60:54:17.5	L	1.396	-	-	-	-	-	-	
ATHDFS_J223317.5-605416A	22:33:17.56	-60:54:16.2	L	7.754	-	-	-	-	-	-	
ATHDFS_J223317.5-605416B	22:33:16.46	-60:54:10.2	L	5.570	-	-	-	-	-	-	
ATHDFS_J223156.0-605417	22:31:56.00	-60:54:17.3	L	0.341	-	-	-	-	-	-	
ATHDFS_J223204.8-605414	22:32:04.87	-60:54:14.6	L	0.526	-	-	-	-	-	-	
ATHDFS_J223228.8-605406	22:32:28.80	-60:54:06.5	L	0.159	-	-	-	-	-	-	
ATHDFS_J223430.9-605357	22:34:30.90	-60:53:57.9	L	0.199	-	-	-	-	-	-	
ATHDFS_J223230.3-605352	22:32:30.30	-60:53:52.1	L	0.289	-	-	-	-	-	-	
ATHDFS_J223151.1-605328	22:31:51.13	-60:53:28.1	L	0.316	-	-	-	-	-	-	
ATHDFS_J223145.4-605311	22:31:45.49	-60:53:11.3	L	0.589	-	-	-	-	-	-	
ATHDFS_J223453.4-605259	22:34:53.47	-60:52:59.9	L	0.483	-	-	-	-	-	-	
ATHDFS_J223141.5-605302	22:31:41.51	-60:53:02.1	L	0.204	-	-	-	-	-	-	
ATHDFS_J223150.6-605258	22:31:50.63	-60:52:58.1	L	0.315	-	-	-	-	-	-	
ATHDFS_J223203.0-605242A	22:32:03.02	-60:52:42.9	L	87.888	-	-	-	-	-	-	
ATHDFS_J223203.0-605242B	22:32:01.80	-60:52:25.8	L	1.239	-	-	-	-	-	-	
ATHDFS_J223301.5-605250A	22:33:01.52	-60:52:50.6	L	0.404	-	-	-	-	-	-	
ATHDFS_J223301.5-605250B	22:33:01.12	-60:52:39.9	L	0.335	-	-	-	-	-	-	
ATHDFS_J223458.6-605225	22:34:58.63	-60:52:25.1	L	5.440	-	-	-	-	-	-	
ATHDFS_J223345.4-605227	22:33:45.46	-60:52:27.4	L	0.111	-	-	-	-	-	-	
ATHDFS_J223454.9-605211	22:34:54.95	-60:52:11.4	L	5.062	-	-	-	-	-	-	
ATHDFS_J223352.5-605210	22:33:52.50	-60:52:10.5	L	0.157	-	-	-	-	-	-	
ATHDFS_J223241.8-605209	22:32:41.85	-60:52:09.3	L	0.094	-	-	-	-	-	-	
ATHDFS_J223242.9-605155	22:32:42.95	-60:51:55.7	L	0.114	-	-	-	-	-	-	
ATHDFS_J223223.3-605137	22:32:23.33	-60:51:37.9	L	2.079	-	-	-	-	-	-	
ATHDFS_J223323.8-605141	22:33:23.89	-60:51:41.5	L	0.114	-	-	-	-	-	-	
ATHDFS_J223420.1-605138	22:34:20.12	-60:51:38.9	L	0.094	-	-	-	-	-	-	
ATHDFS_J223427.0-605132	22:34:27.08	-60:51:32.9	L	0.172	-	-	-	-	-	-	
ATHDFS_J223238.8-605113	22:32:38.89	-60:51:13.8	L	0.086	-	-	-	-	-	-	
ATHDFS_J223403.1-605101	22:34:03.19	-60:51:01.8	L	12.043	-	-	-	-	-	-	
ATHDFS_J223139.6-605039	22:31:39.62	-60:50:39.3	L	0.212	-	-	-	-	-	-	
ATHDFS_J223257.0-605039	22:32:57.01	-60:50:39.1	L	0.120	-	-	-	-	-	-	
ATHDFS_J223226.9-605029	22:32:26.90	-60:50:29.4	L	0.094	-	-	-	-	-	-	
ATHDFS_J223142.8-605024	22:31:42.80	-60:50:24.9	L	0.283	-	-	-	-	-	-	
ATHDFS_J223238.5-605018	22:32:38.56	-60:50:18.5	L	0.405	-	-	-	-	-	-	
ATHDFS_J223306.7-605014	22:33:06.74	-60:50:14.7	L	0.075	-	-	-	-	-	-	
ATHDFS_J223411.6-604931	22:34:11.61	-60:49:31.2	L	0.160	-	-	-	-	-	-	

Table 9—Continued

source name	RA	Dec	Coord Flag	$S_{1.4\text{GHz}}$	$S_{2.5\text{GHz}}$	$S_{5.2\text{GHz}}$	$S_{8.7\text{GHz}}$	$\alpha_{1.4\text{GHz}}^{2.5\text{GHz}}$	$\alpha_{2.5\text{GHz}}^{5.2\text{GHz}}$	$\alpha_{5.2\text{GHz}}^{8.7\text{GHz}}$	AGN flag
ATHDFS_J223329.3–604931	22:33:29.36	–60:49:31.7	L	0.182	<0.15	-	-	<-0.32	-	-	
ATHDFS_J223221.3–604929	22:32:21.37	–60:49:29.1	L	0.083	-	-	-	-	-	-	
ATHDFS_J223223.6–604923	22:32:23.67	–60:49:23.8	L	0.209	-	-	-	-	-	-	
ATHDFS_J223301.3–604926	22:33:01.31	–60:49:26.6	L	0.074	<0.15	-	-	<1.27	-	-	
ATHDFS_J223414.3–604923	22:34:14.39	–60:49:23.4	L	0.134	-	-	-	-	-	-	
ATHDFS_J223524.8–604918A	22:35:24.89	–60:49:18.6	L	0.136	-	-	-	-	-	-	
ATHDFS_J223524.8–604918B	22:35:25.98	–60:49:07.8	L	0.320	-	-	-	-	-	-	
ATHDFS_J223430.0–604922	22:34:30.01	–60:49:22.1	L	0.172	-	-	-	-	-	-	
ATHDFS_J223454.0–604904	22:34:54.04	–60:49:04.6	L	0.483	-	-	-	-	-	-	
ATHDFS_J223413.1–604909	22:34:13.15	–60:49:09.8	L	0.185	-	-	-	-	-	-	
ATHDFS_J223502.1–604858	22:35:02.16	–60:48:58.6	L	0.423	-	-	-	-	-	-	
ATHDFS_J223107.4–604855	22:31:07.48	–60:48:55.0	L	11.272	-	-	-	-	-	-	
ATHDFS_J223400.5–604903A	22:34:00.52	–60:49:03.7	L	0.338	(0.117)	-	-	$-2.29 \pm 0.28$	-	-	
ATHDFS_J223400.5–604903B	22:33:59.41	–60:49:01.4	L	0.110	<0.18	-	-	<0.86	-	-	
ATHDFS_J223359.4–604901	22:33:59.41	–60:49:01.4	L	0.154	<0.18	-	-	<0.29	-	-	
ATHDFS_J223417.0–604857	22:34:17.03	–60:48:57.2	L	0.120	-	-	-	-	-	-	
ATHDFS_J223543.9–604838	22:35:43.90	–60:48:38.6	L	0.614	-	-	-	-	-	-	
ATHDFS_J223407.5–604847	22:34:07.53	–60:48:47.6	L	0.079	(0.085)	-	-	$-0.06 \pm 0.39$	-	-	
ATHDFS_J223235.6–604844	22:32:35.65	–60:48:44.7	L	0.103	-	-	-	-	-	-	
ATHDFS_J223447.4–604843	22:34:47.48	–60:48:43.6	L	0.091	-	-	-	-	-	-	
ATHDFS_J223452.0–604834	22:34:52.03	–60:48:34.4	L	0.245	-	-	-	-	-	-	
ATHDFS_J223337.8–604833	22:33:37.83	–60:48:33.9	L	0.322	(0.091)	-	-	$-1.27 \pm 0.26$	-	-	
ATHDFS_J223146.9–604827	22:31:46.97	–60:48:27.9	L	0.120	-	-	-	-	-	-	
ATHDFS_J223255.7–604823	22:32:55.77	–60:48:23.4	L	0.125	(0.178)	-	-	$0.43 \pm 0.33$	-	-	AGN
ATHDFS_J223250.5–604814	22:32:50.50	–60:48:14.8	L	0.103	<0.16	-	-	<0.74	-	-	
ATHDFS_J223109.5–604810	22:31:09.56	–60:48:10.5	L	0.205	-	-	-	-	-	-	
ATHDFS_J223359.7–604806	22:33:59.72	–60:48:06.3	L	0.103	(0.092)	-	-	$0.26 \pm 0.41$	-	-	AGN
ATHDFS_J223243.0–604758	22:32:43.04	–60:47:58.8	L	0.080	(0.103)	-	-	$0.38 \pm 0.42$	-	-	AGN
ATHDFS_J223414.7–604753	22:34:14.73	–60:47:53.9	L	0.410	(0.140)	-	-	$-1.97 \pm 0.27$	-	-	
ATHDFS_J223217.6–604751	22:32:17.63	–60:47:51.6	L	0.082	-	-	-	-	-	-	
ATHDFS_J223417.5–604749	22:34:17.50	–60:47:49.0	L	0.070	<0.20	-	-	<1.81	-	-	
ATHDFS_J223226.8–604745	22:32:26.84	–60:47:45.5	L	0.186	0.292	-	-	$0.42 \pm 0.29$	-	-	AGN
ATHDFS_J223254.0–604736	22:32:54.06	–60:47:36.8	L	0.336	0.228	-	-	$-0.58 \pm 0.24$	-	-	
ATHDFS_J223340.2–604730	22:33:40.22	–60:47:30.7	L	0.065	<0.14	-	-	<1.25	-	-	
ATHDFS_J223141.7–604725	22:31:41.79	–60:47:25.7	L	0.137	-	-	-	-	-	-	
ATHDFS_J223353.3–604723	22:33:53.32	–60:47:23.6	L	0.075	<0.14	-	-	<1.11	-	-	
ATHDFS_J223527.5–604714	22:35:27.50	–60:47:14.1	L	0.334	-	-	-	-	-	-	
ATHDFS_J223444.0–604710	22:34:44.00	–60:47:10.8	L	0.251	-	-	-	-	-	-	
ATHDFS_J223108.1–604706	22:31:08.16	–60:47:06.9	L	0.192	-	-	-	-	-	-	
ATHDFS_J223315.8–604707	22:33:15.84	–60:47:07.1	L	0.073	<0.14	-	-	<1.10	-	-	
ATHDFS_J223420.4–604658	22:34:20.47	–60:46:58.9	L	0.155	<0.16	-	-	<0.01	-	-	
ATHDFS_J223527.8–604639A	22:35:27.84	–60:46:39.3	L	5.478	-	-	-	-	-	-	
ATHDFS_J223527.8–604639B	22:35:27.35	–60:46:47.3	L	1.423	-	-	-	-	-	-	
ATHDFS_J223231.6–604654	22:32:31.69	–60:46:54.2	L	0.066	<0.18	-	-	<1.66	-	-	
ATHDFS_J223254.0–604650	22:32:54.02	–60:46:50.6	L	0.140	<0.11	-	-	<-0.36	-	-	
ATHDFS_J223147.2–604647	22:31:47.29	–60:46:47.9	L	0.077	-	-	-	-	-	-	
ATHDFS_J223305.3–604647	22:33:05.31	–60:46:47.2	L	0.086	<0.10	-	-	<0.22	-	-	
ATHDFS_J223118.9–604644	22:31:18.99	–60:46:44.0	L	0.174	-	-	-	-	-	-	
ATHDFS_J223333.2–604642	22:33:33.20	–60:46:42.8	L	0.255	0.234	-	-	$0.07 \pm 0.34$	-	-	AGN
ATHDFS_J223300.3–604640	22:33:00.32	–60:46:40.8	L	0.104	<0.12	-	-	<0.24	-	-	
ATHDFS_J223228.5–604642	22:32:28.53	–60:46:42.6	L	0.077	<0.18	-	-	<1.43	-	-	

Table 9—Continued

source name	RA	Dec	Coord Flag	S <sub>1.4GHz</sub>	S <sub>2.5GHz</sub>	S <sub>5.2GHz</sub>	S <sub>8.7GHz</sub>	$\alpha_{1.4GHz}^{2.5GHz}$	$\alpha_{2.5GHz}^{5.2GHz}$	$\alpha_{5.2GHz}^{8.7GHz}$	AGN flag
ATHDFS_J223536.8-604632	22:35:36.87	-60:46:32.7	L	0.568	-	-	-	-	-	-	
ATHDFS_J223312.3-604630	22:33:12.39	-60:46:30.6	L	0.086	<0.12	-	-	<0.59	-	-	
ATHDFS_J223330.4-604624	22:33:30.48	-60:46:24.4	L	0.113	(0.125)	-	-	0.16 ± 0.32	-	-	AGN
ATHDFS_J223434.7-604603	22:34:34.72	-60:46:03.0	L	0.147	(0.179)	-	-	-0.03 ± 0.38	-	-	
ATHDFS_J223310.2-604601	22:33:10.29	-60:46:01.3	L	0.090	<0.12	-	-	<0.51	-	-	
ATHDFS_J223258.6-604548	22:32:58.62	-60:45:48.8	L	0.110	<0.12	-	-	<0.17	-	-	
ATHDFS_J223329.6-604537	22:33:29.69	-60:45:37.4	L	0.272	0.139	-	-	-0.95 ± 0.43	-	-	
ATHDFS_J223408.1-604534	22:34:08.13	-60:45:34.6	L	0.181	(0.060)	-	-	-1.82 ± 0.29	-	-	
ATHDFS_J223342.9-604524	22:33:42.92	-60:45:24.8	L	1.968	1.588	-	-	-0.36 ± 0.03	-	-	
ATHDFS_J223324.0-604516	22:33:24.08	-60:45:16.2	L	0.284	<0.12	-	-	<-1.45	-	-	
ATHDFS_J223320.1-604457	22:33:20.15	-60:44:57.4	L	0.344	<0.13	-	-	<-1.67	-	-	
ATHDFS_J223443.3-604452	22:34:43.38	-60:44:52.7	L	1.534	1.673	-	-	0.18 ± 0.05	-	-	AGN
ATHDFS_J223121.4-604448	22:31:21.45	-60:44:48.5	L	0.131	-	-	-	-	-	-	
ATHDFS_J223311.5-604449	22:33:11.53	-60:44:49.7	L	0.261	(0.091)	-	-	-2.12 ± 0.28	-	-	
ATHDFS_J223319.1-604428	22:33:19.12	-60:44:28.2	L	6.230	5.969	-	-	-0.06 ± 0.01	-	-	AGN
ATHDFS_J223210.3-604433	22:32:10.36	-60:44:33.0	L	56.513	43.478	-	-	-0.45 ± 0.00	-	-	
ATHDFS_J223439.0-604435	22:34:39.08	-60:44:35.4	L	0.184	(0.110)	-	-	-0.51 ± 0.31	-	-	
ATHDFS_J223356.9-604438	22:33:56.94	-60:44:38.9	L	0.085	<0.15	-	-	<0.93	-	-	
ATHDFS_J223244.1-604437	22:32:44.10	-60:44:37.3	L	0.118	(0.239)	-	-	0.20 ± 0.31	-	-	AGN
ATHDFS_J223147.2-604415	22:31:47.29	-60:44:15.2	L	0.091	-	-	-	-	-	-	
ATHDFS_J223326.3-604416	22:33:26.38	-60:44:16.4	L	0.089	<0.12	-	-	<0.46	-	-	
ATHDFS_J223255.2-604415	22:32:55.26	-60:44:15.7	L	0.069	<0.10	-	-	<0.66	-	-	
ATHDFS_J223422.4-604412	22:34:22.41	-60:44:12.0	L	0.130	(0.078)	-	-	-1.13 ± 0.36	-	-	
ATHDFS_J223226.8-604408	22:32:26.88	-60:44:08.8	L	0.133	<0.13	-	-	<-0.05	-	-	
ATHDFS_J223313.9-604359	22:33:13.90	-60:43:59.8	L	0.175	<0.12	-	-	<-0.59	-	-	
ATHDFS_J223255.6-604400	22:32:55.65	-60:44:00.1	L	0.101	0.191	-	-	0.77 ± 0.33	-	-	AGN
ATHDFS_J223101.3-604351	22:31:01.30	-60:43:51.4	L	0.159	-	-	-	-	-	-	
ATHDFS_J223319.1-604348	22:33:19.13	-60:43:48.6	L	1.085	0.691	-	-	-0.59 ± 0.09	-	-	
ATHDFS_J223147.4-604338	22:31:47.48	-60:43:38.2	L	0.176	-	-	-	-	-	-	
ATHDFS_J223126.2-604337	22:31:26.24	-60:43:37.3	L	0.174	-	-	-	-	-	-	
ATHDFS_J223439.7-604337	22:34:39.73	-60:43:37.3	L	0.211	<0.17	-	-	<-0.37	-	-	
ATHDFS_J223534.3-604328	22:35:34.32	-60:43:28.9	L	0.657	-	-	-	-	-	-	
ATHDFS_J223250.6-604336	22:32:50.62	-60:43:36.5	L	0.105	<0.11	-	-	<0.08	-	-	
ATHDFS_J223522.2-604326	22:35:22.26	-60:43:26.9	L	0.222	-	-	-	-	-	-	
ATHDFS_J223330.4-604332	22:33:30.46	-60:43:32.5	L	0.080	<0.12	-	-	<0.71	-	-	
ATHDFS_J223355.6-604315	22:33:55.63	-60:43:15.7	L	154.700	111.800	-	-	-0.53 ± 0.00	-	-	
ATHDFS_J223440.4-604309	22:34:40.46	-60:43:09.9	L	0.150	<0.20	-	-	<0.49	-	-	
ATHDFS_J223430.8-604310	22:34:30.82	-60:43:10.4	L	0.141	<0.16	-	-	<0.25	-	-	
ATHDFS_J223240.2-604306	22:32:40.24	-60:43:06.5	L	0.091	(0.098)	-	-	-0.26 ± 0.31	-	-	
ATHDFS_J223207.9-604305	22:32:07.96	-60:43:05.6	L	0.114	<0.18	-	-	<0.73	-	-	
ATHDFS_J223427.3-604258	22:34:27.34	-60:42:58.8	S	0.571	0.596	-	-	0.00 ± 0.11	-	-	AGN
ATHDFS_J223130.4-604232	22:31:30.45	-60:42:32.3	L	0.235	-	-	-	-	-	-	
ATHDFS_J223425.8-604232	22:34:25.82	-60:42:32.7	L	0.137	(0.129)	-	-	0.21 ± 0.50	-	-	AGN
ATHDFS_J223239.0-604230	22:32:39.04	-60:42:30.1	L	0.056	<0.09	-	-	<0.82	-	-	
ATHDFS_J223312.4-604227	22:33:12.45	-60:42:27.2	L	0.078	0.137	-	-	0.77 ± 0.38	-	-	AGN
ATHDFS_J223437.2-604214	22:34:37.27	-60:42:14.3	L	2.872	3.876	-	-	0.55 ± 0.02	-	-	AGN
ATHDFS_J223508.5-604217	22:35:08.52	-60:42:17.5	L	0.173	-	-	-	-	-	-	
ATHDFS_J223338.8-604216	22:33:38.89	-60:42:16.4	L	0.168	0.132	-	-	0.04 ± 0.34	-	-	AGN
ATHDFS_J223523.6-604207	22:35:23.69	-60:42:07.9	L	0.723	-	-	-	-	-	-	
ATHDFS_J223135.8-604207	22:31:35.84	-60:42:07.0	L	0.113	-	-	-	-	-	-	
ATHDFS_J223359.8-604155	22:33:59.86	-60:41:55.4	S	0.536	0.162	-	-	-1.11 ± 0.39	-	-	



Table 9—Continued

source name	RA	Dec	Coord Flag	$S_{1.4\text{GHz}}$	$S_{2.5\text{GHz}}$	$S_{5.2\text{GHz}}$	$S_{8.7\text{GHz}}$	$\alpha_{1.4\text{GHz}}^{2.5\text{GHz}}$	$\alpha_{2.5\text{GHz}}^{5.2\text{GHz}}$	$\alpha_{5.2\text{GHz}}^{8.7\text{GHz}}$	AGN flag
ATHDFS_J223255.4–604151	22:32:55.45	–60:41:51.3	L	0.132	(0.046)	-	-	$-1.38 \pm 0.31$	-	-	
ATHDFS_J223158.4–604142	22:31:58.45	–60:41:42.3	L	0.111	<0.13	-	-	<0.31	-	-	
ATHDFS_J223339.5–604131	22:33:39.59	–60:41:31.1	L	0.094	(0.048)	-	-	$-1.36 \pm 0.35$	-	-	
ATHDFS_J223224.5–604113	22:32:24.52	–60:41:13.0	L	4.108	3.052	-	-	$-0.48 \pm 0.02$	-	-	
ATHDFS_J223206.5–604102	22:32:06.53	–60:41:02.2	L	0.073	<0.15	-	-	<1.19	-	-	
ATHDFS_J223448.3–604042	22:34:48.33	–60:40:42.8	L	0.437	0.290	-	-	$-0.54 \pm 0.30$	-	-	
ATHDFS_J223430.1–604043	22:34:30.13	–60:40:43.5	L	0.057	<0.10	-	-	<0.88	-	-	
ATHDFS_J223251.1–604042	22:32:51.14	–60:40:42.1	L	0.070	<0.09	-	-	<0.36	-	-	
ATHDFS_J223514.4–604024	22:35:14.48	–60:40:24.8	L	0.238	-	-	-	-	-	-	
ATHDFS_J223348.2–604026	22:33:48.25	–60:40:26.7	L	0.097	(0.047)	-	-	$-1.25 \pm 0.35$	-	-	
ATHDFS_J223429.8–604020	22:34:29.84	–60:40:20.2	L	0.099	(0.159)	-	-	$0.43 \pm 0.32$	-	-	AGN
ATHDFS_J223417.8–604009	22:34:17.80	–60:40:09.3	L	1.502	1.092	-	-	$-0.47 \pm 0.05$	-	-	
ATHDFS_J223337.5–604006	22:33:37.53	–60:40:06.6	L	0.094	<0.10	-	-	<0.02	-	-	
ATHDFS_J223412.2–603957	22:34:12.22	–60:39:57.3	L	0.083	<0.08	-	-	<0.02	-	-	
ATHDFS_J223438.0–603951	22:34:38.07	–60:39:51.2	L	0.102	(0.074)	-	-	$-0.84 \pm 0.35$	-	-	
ATHDFS_J223343.9–603953	22:33:43.91	–60:39:53.6	L	0.102	<0.09	-	-	<-0.26	-	-	
ATHDFS_J223047.9–603933	22:30:47.91	–60:39:33.7	L	0.239	-	-	-	-	-	-	
ATHDFS_J223324.7–603934	22:33:24.71	–60:39:34.6	L	0.092	(0.059)	-	-	$-0.69 \pm 0.33$	-	-	
ATHDFS_J223220.6–603931	22:32:20.60	–60:39:31.8	L	0.138	0.136	-	-	$-0.25 \pm 0.34$	-	-	
ATHDFS_J223529.2–603927	22:35:29.20	–60:39:27.0	L	0.229	-	-	-	-	-	-	
ATHDFS_J223400.2–603930	22:34:00.27	–60:39:30.4	L	0.117	<0.08	-	-	<-0.74	-	-	
ATHDFS_J223207.9–603928	22:32:07.99	–60:39:28.7	L	0.107	(0.205)	-	-	$0.20 \pm 0.34$	-	-	AGN
ATHDFS_J223222.7–603924	22:32:22.72	–60:39:24.4	L	0.086	<0.09	-	-	<0.10	-	-	
ATHDFS_J223253.7–603921	22:32:53.70	–60:39:21.2	L	0.052	<0.07	-	-	<0.48	-	-	
ATHDFS_J223331.3–603914	22:33:31.32	–60:39:14.6	L	0.099	<0.08	-	-	<-0.32	-	-	
ATHDFS_J223123.1–603903	22:31:23.18	–60:39:03.5	L	23.988	-	-	-	-	-	-	
ATHDFS_J223258.7–603903	22:32:58.79	–60:39:03.9	L	0.058	(0.033)	-	-	$-0.96 \pm 0.37$	-	-	
ATHDFS_J223245.6–603857	22:32:45.65	–60:38:57.3	L	0.843	0.536	-	-	$-0.69 \pm 0.06$	-	-	
ATHDFS_J223205.9–603857	22:32:05.99	–60:38:57.0	L	0.286	0.222	-	-	$-0.80 \pm 0.29$	-	-	
ATHDFS_J223144.4–603858	22:31:44.45	–60:38:58.4	L	0.107	-	-	-	-	-	-	
ATHDFS_J223153.7–603853	22:31:53.74	–60:38:53.6	L	0.076	<0.14	-	-	<1.07	-	-	
ATHDFS_J223450.4–603844	22:34:50.40	–60:38:44.9	L	0.212	(0.070)	-	-	$-1.87 \pm 0.29$	-	-	
ATHDFS_J223307.1–603846	22:33:07.13	–60:38:46.9	L	0.137	0.074	-	-	$-1.00 \pm 0.43$	-	-	
ATHDFS_J223457.3–603840	22:34:57.30	–60:38:40.2	L	0.184	(0.128)	-	-	$-0.46 \pm 0.36$	-	-	
ATHDFS_J223232.3–603842	22:32:32.32	–60:38:42.3	L	0.085	(0.076)	-	-	$-0.36 \pm 0.35$	-	-	
ATHDFS_J223335.9–603828	22:33:35.94	–60:38:28.4	S	-	0.092	-	-	-	-	-	
ATHDFS_J223505.5–603825	22:35:05.53	–60:38:25.9	L	0.343	<0.06	-	-	-	-	-	
ATHDFS_J223304.6–603835	22:33:04.66	–60:38:35.8	L	0.067	-	-	-	<-0.14	-	-	
ATHDFS_J223608.1–603823	22:36:08.12	–60:38:23.9	L	0.258	-	-	-	-	-	-	
ATHDFS_J223432.1–603815	22:34:32.16	–60:38:15.0	S	0.268	0.371	-	-	$0.65 \pm 0.20$	-	-	AGN
ATHDFS_J223138.7–603818	22:31:38.74	–60:38:18.5	L	0.089	-	-	-	-	-	-	
ATHDFS_J223418.6–603808	22:34:18.63	–60:38:08.0	L	0.346	0.244	-	-	$-0.33 \pm 0.15$	-	-	
ATHDFS_J223442.7–603802	22:34:42.70	–60:38:02.4	L	0.254	0.215	-	-	$-0.51 \pm 0.31$	-	-	
ATHDFS_J223248.2–603805	22:32:48.29	–60:38:05.6	L	0.076	(0.060)	<0.10	-	$-0.48 \pm 0.34$	-	-	
ATHDFS_J223334.4–603804	22:33:34.47	–60:38:04.7	L	0.064	<0.07	-	-	<0.15	-	-	
ATHDFS_J223436.9–603754	22:34:36.90	–60:37:54.6	L	0.553	0.453	-	-	$-0.30 \pm 0.11$	-	-	
ATHDFS_J223346.9–603753	22:33:46.98	–60:37:53.5	S	-	0.076	-	-	-	-	-	
ATHDFS_J223254.5–603748	22:32:54.53	–60:37:48.0	L	0.092	<0.08	<0.10	-	<-0.34	-	-	
ATHDFS_J223350.0–603741	22:33:50.09	–60:37:41.3	L	0.670	0.543	-	-	$-0.36 \pm 0.05$	-	-	
ATHDFS_J223441.6–603740	22:34:41.61	–60:37:40.3	L	0.194	(0.079)	-	-	$-1.07 \pm 0.29$	-	-	
ATHDFS_J223232.8–603737	22:32:32.85	–60:37:37.1	L	0.645	0.489	0.280	-	$-0.51 \pm 0.08$	$-0.98 \pm 0.19$	-	

Table 9—Continued

source name	RA	Dec	Coord Flag	$S_{1.4\text{GHz}}$	$S_{2.5\text{GHz}}$	$S_{5.2\text{GHz}}$	$S_{8.7\text{GHz}}$	$\alpha_{1.4\text{GHz}}^{2.5\text{GHz}}$	$\alpha_{2.5\text{GHz}}^{5.2\text{GHz}}$	$\alpha_{5.2\text{GHz}}^{8.7\text{GHz}}$	AGN flag
ATHDFS_J223142.5-603737	22:31:42.51	-60:37:37.4	L	0.213	-	-	-	-	-	-	
ATHDFS_J223404.8-603732	22:34:04.84	-60:37:32.3	L	3.238	2.158	-	-	$-0.66 \pm 0.03$	-	-	
ATHDFS_J223503.2-603729	22:35:03.21	-60:37:29.2	L	0.064	$<0.14$	-	-	$<1.28$	-	-	
ATHDFS_J223437.7-603726	22:34:37.73	-60:37:26.5	L	0.187	(0.090)	-	-	$-0.93 \pm 0.28$	-	-	
ATHDFS_J223417.1-603724	22:34:17.18	-60:37:24.5	L	0.157	(0.081)	-	-	$-1.26 \pm 0.30$	-	-	
ATHDFS_J223341.2-603724	22:33:41.20	-60:37:24.7	L	0.071	(0.089)	-	-	$0.19 \pm 0.42$	-	-	AGN
ATHDFS_J223225.6-603717	22:32:25.68	-60:37:17.4	L	0.061	$<0.09$	-	-	$<0.73$	-	-	
ATHDFS_J223202.5-603714	22:32:02.55	-60:37:14.0	L	0.151	(0.103)	-	-	$-0.62 \pm 0.28$	-	-	
ATHDFS_J223326.0-603716	22:33:26.01	-60:37:16.7	L	0.083	$<0.07$	-	-	$<-0.34$	-	-	
ATHDFS_J223506.5-603700	22:35:06.52	-60:37:00.3	L	0.088	-	-	-	-	-	-	
ATHDFS_J223236.6-603657	22:32:36.60	-60:36:57.7	S	-	0.111	-	-	-	-	-	
ATHDFS_J223400.2-603653	22:34:00.29	-60:36:53.3	L	2.209	1.399	-	-	$-0.77 \pm 0.03$	-	-	
ATHDFS_J223525.8-603652	22:35:25.88	-60:36:52.0	L	0.135	-	-	-	-	-	-	
ATHDFS_J223343.7-603651	22:33:43.76	-60:36:51.5	L	0.070	(0.040)	-	-	$-1.14 \pm 0.39$	-	-	
ATHDFS_J223404.3-603638	22:34:04.36	-60:36:38.8	L	1.050	0.743	-	-	$-0.63 \pm 0.06$	-	-	
ATHDFS_J223158.1-603636	22:31:58.14	-60:36:36.7	L	0.173	(0.078)	-	-	$-1.21 \pm 0.29$	-	-	
ATHDFS_J223605.7-603631	22:36:05.78	-60:36:31.0	L	0.148	-	-	-	-	-	-	
ATHDFS_J223406.7-603637	22:34:06.76	-60:36:37.6	L	0.127	(0.040)	-	-	$-1.14 \pm 0.34$	-	-	
ATHDFS_J223054.4-603631	22:30:54.42	-60:36:31.5	L	0.177	-	-	-	-	-	-	
ATHDFS_J223439.9-603629	22:34:39.95	-60:36:29.7	L	0.407	$<0.13$	-	-	$<-1.92$	-	-	
ATHDFS_J223341.9-603634	22:33:41.93	-60:36:34.5	L	0.174	(0.098)	-	-	$-0.83 \pm 0.31$	-	-	
ATHDFS_J223451.7-603632	22:34:51.76	-60:36:32.9	L	0.066	(0.194)	-	-	$1.56 \pm 0.33$	-	-	AGN
ATHDFS_J223429.9-603629	22:34:29.97	-60:36:29.6	L	0.671	0.785	-	-	$0.35 \pm 0.06$	-	-	AGN
ATHDFS_J223316.5-603627	22:33:16.55	-60:36:27.5	L	0.661	0.451	0.204	-	$-0.67 \pm 0.06$	$-1.03 \pm 0.19$	-	
ATHDFS_J223526.2-603617	22:35:26.21	-60:36:17.6	L	0.190	-	-	-	-	-	-	
ATHDFS_J223518.7-603619	22:35:18.73	-60:36:19.9	L	0.094	-	-	-	-	-	-	
ATHDFS_J223456.2-603619	22:34:56.21	-60:36:19.2	L	0.120	(0.089)	-	-	$0.12 \pm 0.32$	-	-	AGN
ATHDFS_J223158.5-603614	22:31:58.59	-60:36:14.1	L	0.094	$<0.14$	-	-	$<0.66$	-	-	
ATHDFS_J223410.3-603613	22:34:10.31	-60:36:13.4	L	0.088	$<0.09$	-	-	$<-0.04$	-	-	
ATHDFS_J223421.8-603603	22:34:21.85	-60:36:03.8	L	0.068	$<0.09$	-	-	$<0.47$	-	-	
ATHDFS_J223232.4-603542A	22:32:32.40	-60:35:42.5	L	0.529	0.334	0.115	-	$-1.43 \pm 0.34$	$-0.60 \pm 0.38$	-	
ATHDFS_J223232.4-603542B	22:32:32.56	-60:35:53.1	L	0.466	0.236	0.141	-	$-1.56 \pm 0.37$	$-0.35 \pm 0.38$	-	
ATHDFS_J223104.8-603549	22:31:04.80	-60:35:49.2	L	0.162	-	-	-	-	-	-	
ATHDFS_J223525.7-603544	22:35:25.76	-60:35:44.2	L	0.415	-	-	-	-	-	-	
ATHDFS_J223229.8-603544	22:32:29.89	-60:35:44.9	L	0.087	(0.060)	$<0.09$	-	$-0.42 \pm 0.35$	-	-	
ATHDFS_J223422.0-603544	22:34:22.07	-60:35:44.1	S	-	0.070	-	-	-	-	-	
ATHDFS_J223224.0-603537	22:32:24.02	-60:35:37.7	L	1.259	0.836	0.396	-	$-0.66 \pm 0.05$	$-0.94 \pm 0.10$	-	
ATHDFS_J223253.0-603539	22:32:53.09	-60:35:39.7	L	0.091	(0.066)	(0.036)	$<0.10$	$-1.14 \pm 0.32$	$-0.08 \pm 0.29$	-	
ATHDFS_J223459.4-603535	22:34:59.48	-60:35:35.7	L	0.094	$<0.18$	-	-	$<1.06$	-	-	
ATHDFS_J223245.3-603537	22:32:45.34	-60:35:37.8	L	0.051	$<0.08$	$<0.05$	$<0.13$	$<0.65$	-	-	
ATHDFS_J223046.1-603525	22:30:46.14	-60:35:25.0	L	0.502	-	-	-	-	-	-	
ATHDFS_J223435.5-603532	22:34:35.51	-60:35:32.1	L	0.149	(0.096)	-	-	$-0.24 \pm 0.33$	-	-	
ATHDFS_J223338.8-603523	22:33:38.84	-60:35:23.8	L	0.197	0.159	-	-	$-0.35 \pm 0.21$	-	-	
ATHDFS_J223208.3-603519	22:32:08.36	-60:35:19.2	L	0.918	0.551	-	-	$-0.67 \pm 0.09$	-	-	
ATHDFS_J223223.7-603520	22:32:23.70	-60:35:20.5	L	0.142	$<0.09$	$<0.09$	-	$<-0.82$	-	-	
ATHDFS_J223344.9-603515	22:33:44.99	-60:35:15.6	L	0.344	0.211	-	-	$-0.52 \pm 0.21$	-	-	
ATHDFS_J223524.8-603509	22:35:24.81	-60:35:09.6	L	0.131	-	-	-	-	-	-	
ATHDFS_J223536.3-603506	22:35:36.36	-60:35:06.4	L	0.101	-	-	-	-	-	-	
ATHDFS_J223410.1-603510	22:34:10.15	-60:35:10.2	S	0.064	0.087	-	-	$0.34 \pm 0.44$	-	-	AGN
ATHDFS_J223549.5-603502	22:35:49.56	-60:35:02.4	L	0.151	-	-	-	-	-	-	
ATHDFS_J223350.5-603503	22:33:50.53	-60:35:03.9	L	1.252	0.724	-	-	$-0.85 \pm 0.05$	-	-	

Table 9—Continued

source name	RA	Dec	Coord Flag	$S_{1.4\text{GHz}}$	$S_{2.5\text{GHz}}$	$S_{5.2\text{GHz}}$	$S_{8.7\text{GHz}}$	$\alpha_{1.4\text{GHz}}^{2.5\text{GHz}}$	$\alpha_{2.5\text{GHz}}^{5.2\text{GHz}}$	$\alpha_{5.2\text{GHz}}^{8.7\text{GHz}}$	AGN flag
ATHDFS_J223229.2–603459A	22:32:29.21	–60:34:59.5	L	0.204	(0.110)	(0.080)	-	$-1.22 \pm 0.27$	$0.01 \pm 0.29$	-	
ATHDFS_J223229.2–603459B	22:32:30.21	–60:35:03.5	C	0.149	0.128	0.083	-	$-0.09 \pm 0.32$	$-0.65 \pm 0.47$	-	
ATHDFS_J223541.5–603454	22:35:41.59	–60:34:54.7	L	0.274	-	-	-	-	-	-	
ATHDFS_J223438.6–603450	22:34:38.60	–60:34:50.4	L	3.670	2.776	-	-	$-0.40 \pm 0.02$	-	-	
ATHDFS_J223103.2–603453	22:31:03.28	–60:34:53.7	L	0.107	-	-	-	-	-	-	
ATHDFS_J223116.4–603452	22:31:16.41	–60:34:52.0	L	0.149	-	-	-	-	-	-	
ATHDFS_J223431.8–603454	22:34:31.81	–60:34:54.7	L	0.101	(0.098)	-	-	$-0.51 \pm 0.38$	-	-	
ATHDFS_J223425.0–603452	22:34:25.00	–60:34:52.7	L	0.145	(0.101)	-	-	$-1.24 \pm 0.28$	-	-	
ATHDFS_J223212.3–603448	22:32:12.39	–60:34:48.7	L	0.093	<0.12	-	-	<0.45	-	-	
ATHDFS_J223307.1–603448	22:33:07.18	–60:34:48.8	L	0.103	<0.07	<0.05	<0.09	<-0.58	-	-	
ATHDFS_J223207.4–603445	22:32:07.49	–60:34:45.8	L	0.066	<0.13	-	-	<1.12	-	-	
ATHDFS_J223243.3–603443	22:32:43.32	–60:34:42.5	C	0.063	<0.07	0.053	<0.09	<0.21	-	-	
ATHDFS_J223410.6–603437	22:34:10.65	–60:34:37.7	L	0.080	<0.08	-	-	<0.01	-	-	
ATHDFS_J223442.8–603433	22:34:42.84	–60:34:33.9	L	0.068	<0.12	-	-	<0.98	-	-	
ATHDFS_J223216.6–603434	22:32:16.63	–60:34:34.9	L	0.070	<0.11	<0.10	-	<0.75	-	-	
ATHDFS_J223539.3–603424	22:35:39.39	–60:34:24.7	L	0.189	-	-	-	-	-	-	
ATHDFS_J223153.2–603422	22:31:53.25	–60:34:22.8	L	0.221	(0.079)	-	-	$-2.17 \pm 0.28$	-	-	
ATHDFS_J223401.0–603424	22:34:01.00	–60:34:24.4	L	0.122	(0.043)	-	-	$-2.03 \pm 0.33$	-	-	
ATHDFS_J223245.5–603419	22:32:45.51	–60:34:19.0	C	0.265	0.161	0.060	(0.075)	$-0.43 \pm 0.21$	$-1.44 \pm 0.33$	$0.15 \pm 0.41$	
ATHDFS_J223231.6–603423	22:32:31.69	–60:34:23.1	L	0.070	<0.09	(0.059)	<0.15	<0.44	-	-	
ATHDFS_J223055.9–603412	22:30:55.98	–60:34:12.7	L	0.362	-	-	-	-	-	-	
ATHDFS_J223327.6–603414	22:33:27.67	–60:34:14.3	S	0.456	0.498	0.269	-	$0.21 \pm 0.08$	$-0.74 \pm 0.12$	-	GPS
ATHDFS_J223311.9–603417	22:33:11.97	–60:34:17.1	L	0.059	(0.044)	(0.029)	<0.09	$-0.58 \pm 0.38$	$0.25 \pm 0.29$	-	
ATHDFS_J223434.1–603410	22:34:34.17	–60:34:10.1	L	0.086	(0.139)	-	-	$0.30 \pm 0.31$	-	-	AGN
ATHDFS_J223053.2–603402	22:30:53.25	–60:34:02.9	L	0.233	-	-	-	-	-	-	
ATHDFS_J223415.0–603408	22:34:15.00	–60:34:08.6	L	0.054	<0.10	-	-	<1.06	-	-	
ATHDFS_J223529.7–603359	22:35:29.75	–60:33:59.0	L	0.129	-	-	-	-	-	-	
ATHDFS_J223406.6–603401	22:34:06.69	–60:34:01.2	L	0.189	<0.09	-	-	<-1.30	-	-	
ATHDFS_J223409.7–603402	22:34:09.76	–60:34:02.5	L	0.053	<0.09	-	-	<0.94	-	-	
ATHDFS_J223512.7–603353	22:35:12.76	–60:33:53.3	L	0.129	-	-	-	-	-	-	
ATHDFS_J223306.0–603350	22:33:06.07	–60:33:50.3	L	0.452	0.288	0.123	(0.042)	$-0.62 \pm 0.12$	$-1.41 \pm 0.20$	$-1.11 \pm 0.41$	
ATHDFS_J223329.7–603352	22:33:29.74	–60:33:51.9	C	0.152	0.091	0.082	-	$-0.78 \pm 0.41$	$0.37 \pm 0.39$	-	
ATHDFS_J223258.5–603346	22:32:58.59	–60:33:46.7	L	1.010	0.658	0.404	0.260	$-0.65 \pm 0.05$	$-0.76 \pm 0.07$	$-0.82 \pm 0.16$	
ATHDFS_J223243.4–603352	22:32:43.47	–60:33:51.0	X	0.098	(0.054)	0.073	0.114	$-1.30 \pm 0.31$	$0.77 \pm 0.29$	$0.39 \pm 0.48$	
ATHDFS_J223545.7–603342	22:35:45.76	–60:33:42.3	L	0.100	-	-	-	-	-	-	
ATHDFS_J223138.5–603344	22:31:38.52	–60:33:44.7	L	0.097	-	-	-	-	-	-	
ATHDFS_J223420.9–603336	22:34:20.95	–60:33:36.5	L	4.328	2.453	-	-	$-0.94 \pm 0.02$	-	-	
ATHDFS_J223225.0–603338	22:32:25.05	–60:33:38.7	L	0.098	<0.10	<0.06	-	<0.05	-	-	
ATHDFS_J223513.7–603333	22:35:13.73	–60:33:33.3	L	0.113	-	-	-	-	-	-	
ATHDFS_J223247.6–603337	22:32:47.65	–60:33:37.0	L	0.082	<0.08	(0.038)	<0.07	<0.05	-	-	
ATHDFS_J223337.5–603329	22:33:37.57	–60:33:29.1	L	1.126	0.718	0.373	-	$-0.69 \pm 0.05$	$-1.02 \pm 0.11$	-	
ATHDFS_J223253.1–603329	22:32:53.15	–60:33:29.1	L	0.113	(0.054)	<0.04	<0.06	$-1.14 \pm 0.38$	-	-	
ATHDFS_J223302.8–603323	22:33:02.83	–60:33:23.8	L	0.051	<0.08	<0.05	<0.07	<0.73	-	-	
ATHDFS_J223509.5–603257	22:35:09.56	–60:32:57.1	L	0.980	-	-	-	-	-	-	
ATHDFS_J223327.9–603304A	22:33:27.95	–60:33:04.8	L	0.234	0.187	0.114	-	$-0.52 \pm 0.17$	$-0.60 \pm 0.26$	-	
ATHDFS_J223327.9–603304B	22:33:29.28	–60:33:02.0	L	0.059	<0.07	<0.08	-	<0.38	-	-	
ATHDFS_J223306.2–603307	22:33:06.26	–60:33:07.9	X	-	-	-	0.092	-	-	-	
ATHDFS_J223339.4–603306	22:33:39.41	–60:33:06.0	L	0.058	<0.08	<0.10	-	<0.46	-	-	
ATHDFS_J223121.6–603301	22:31:21.62	–60:33:01.1	L	0.075	-	-	-	-	-	-	
ATHDFS_J223242.6–603258	22:32:42.66	–60:32:58.1	X	-	-	-	0.077	-	-	-	
ATHDFS_J223234.2–603257	22:32:34.27	–60:32:57.4	L	0.079	<0.10	<0.05	<0.11	<0.42	-	-	

Table 9—Continued

source name	RA	Dec	Coord Flag	$S_{1.4\text{GHz}}$	$S_{2.5\text{GHz}}$	$S_{5.2\text{GHz}}$	$S_{8.7\text{GHz}}$	$\alpha_{1.4\text{GHz}}^{2.5\text{GHz}}$	$\alpha_{2.5\text{GHz}}^{5.2\text{GHz}}$	$\alpha_{5.2\text{GHz}}^{8.7\text{GHz}}$	AGN flag
ATHDFS_J223308.6–603251	22:33:08.60	–60:32:51.7	L	0.821	0.495	0.196	0.092	$-0.86 \pm 0.03$	$-0.89 \pm 0.11$	$-0.72 \pm 0.43$	
ATHDFS_J223456.8–603251	22:34:56.81	–60:32:51.2	L	0.080	-	-	-	-	-	-	
ATHDFS_J223323.2–603249	22:33:23.25	–60:32:49.2	C	0.460	0.561	0.370	0.223	$0.37 \pm 0.06$	$-0.59 \pm 0.07$	$-0.82 \pm 0.29$	GPS
ATHDFS_J223209.7–603253	22:32:09.71	–60:32:53.9	L	0.061	$<0.12$	-	-	$<1.18$	-	-	
ATHDFS_J223212.9–603234A	22:32:12.90	–60:32:34.6	L	2.816	1.574	0.716	-	$-0.74 \pm 0.05$	$-1.04 \pm 0.09$	-	
ATHDFS_J223212.9–603234B	22:32:12.95	–60:32:43.3	L	1.466	0.903	0.657	-	$-0.51 \pm 0.08$	$-0.98 \pm 0.13$	-	
ATHDFS_J223229.5–603243	22:32:29.55	–60:32:43.6	C	0.254	0.143	0.117	$<0.15$	$-0.86 \pm 0.25$	$-0.38 \pm 0.30$	-	
ATHDFS_J223509.4–603235	22:35:09.44	–60:32:35.9	L	0.583	-	-	-	-	-	-	
ATHDFS_J223142.5–603238	22:31:42.59	–60:32:38.5	L	0.111	-	-	-	-	-	-	
ATHDFS_J223521.1–603235	22:35:21.14	–60:32:35.5	L	0.192	-	-	-	-	-	-	
ATHDFS_J223317.7–603235	22:33:17.75	–60:32:35.2	L	0.070	$<0.08$	(0.037)	$<0.11$	$<0.24$	-	-	
ATHDFS_J223335.3–603234	22:33:35.31	–60:32:34.5	L	0.054	$<0.08$	$<0.08$	-	$<0.65$	-	-	
ATHDFS_J223429.9–603226	22:34:29.99	–60:32:26.9	L	0.075	$<0.11$	-	-	$<0.64$	-	-	
ATHDFS_J223331.6–603222	22:33:31.64	–60:32:22.2	L	0.395	0.286	0.130	-	$-0.68 \pm 0.15$	$-1.05 \pm 0.32$	-	
ATHDFS_J223504.4–603221	22:35:04.47	–60:32:21.1	L	0.129	-	-	-	-	-	-	
ATHDFS_J223343.5–603211	22:33:43.56	–60:32:11.4	L	0.115	$<0.08$	-	-	$<-0.62$	-	-	
ATHDFS_J223302.1–603213	22:33:02.18	–60:32:13.2	L	0.063	$<0.08$	$<0.04$	$<0.07$	$<0.36$	-	-	
ATHDFS_J223519.4–603157A	22:35:19.49	–60:31:57.4	L	0.516	-	-	-	-	-	-	
ATHDFS_J223519.4–603157B	22:35:18.61	–60:31:51.3	L	0.147	-	-	-	-	-	-	
ATHDFS_J223351.1–603153	22:33:51.15	–60:31:53.1	S	-	0.079	-	-	-	-	-	
ATHDFS_J223113.5–603147	22:31:13.53	–60:31:47.0	L	0.831	-	-	-	-	-	-	
ATHDFS_J223433.9–603150	22:34:33.99	–60:31:50.0	L	0.055	$<0.12$	-	-	$<1.32$	-	-	
ATHDFS_J223449.7–603137	22:34:49.78	–60:31:37.8	L	0.069	-	-	-	-	-	-	
ATHDFS_J223303.1–603132	22:33:03.17	–60:31:32.8	L	0.052	(0.055)	(0.035)	$<0.07$	$0.18 \pm 0.39$	$-0.34 \pm 0.29$	-	AGN
ATHDFS_J223254.4–603131	22:32:54.41	–60:31:31.5	L	0.139	(0.059)	(0.035)	$<0.08$	$-1.89 \pm 0.33$	$0.20 \pm 0.29$	-	
ATHDFS_J223316.0–603127	22:33:16.09	–60:31:27.6	L	0.052	$<0.09$	(0.040)	$<0.12$	$<0.89$	-	-	
ATHDFS_J223548.9–603113	22:35:48.99	–60:31:13.5	L	1.357	-	-	-	-	-	-	
ATHDFS_J223201.4–603118	22:32:01.42	–60:31:18.9	L	0.088	-	-	-	-	-	-	
ATHDFS_J223351.7–603117	22:33:51.76	–60:31:17.3	L	0.075	(0.039)	-	-	$-0.78 \pm 0.44$	-	-	
ATHDFS_J223504.6–603109	22:35:04.63	–60:31:09.3	L	0.181	-	-	-	-	-	-	
ATHDFS_J223415.5–603108	22:34:15.51	–60:31:08.3	L	0.075	$<0.12$	-	-	$<0.75$	-	-	
ATHDFS_J223256.4–603058	22:32:56.42	–60:30:58.9	L	0.087	$<0.09$	(0.030)	$<0.09$	$<0.15$	-	-	
ATHDFS_J223550.9–603050	22:35:50.97	–60:30:50.2	L	0.072	-	-	-	-	-	-	
ATHDFS_J223447.4–603050	22:34:47.48	–60:30:50.1	L	0.062	-	-	-	-	-	-	
ATHDFS_J223146.0–603046	22:31:46.03	–60:30:46.6	L	0.099	-	-	-	-	-	-	
ATHDFS_J223345.0–603041	22:33:45.06	–60:30:41.4	L	0.116	(0.060)	-	-	$-0.92 \pm 0.29$	-	-	
ATHDFS_J223404.0–603037A	22:34:04.02	–60:30:37.6	L	0.190	0.122	-	-	$-0.62 \pm 0.38$	-	-	
ATHDFS_J223404.0–603037B	22:34:05.30	–60:30:29.2	L	0.132	(0.070)	-	-	$-0.49 \pm 0.30$	-	-	
ATHDFS_J223445.6–603032	22:34:45.67	–60:30:32.3	L	0.062	-	-	-	-	-	-	
ATHDFS_J223304.8–603031	22:33:04.89	–60:30:31.2	L	0.084	$<0.09$	(0.033)	$<0.11$	$<0.18$	-	-	
ATHDFS_J223120.1–603025	22:31:20.18	–60:30:25.7	L	0.102	-	-	-	-	-	-	
ATHDFS_J223537.7–603013	22:35:37.72	–60:30:13.3	L	2.860	-	-	-	-	-	-	
ATHDFS_J223241.4–603025	22:32:41.42	–60:30:25.9	L	0.092	(0.063)	(0.038)	$<0.15$	$-0.93 \pm 0.30$	$0.25 \pm 0.29$	-	
ATHDFS_J223414.6–603024	22:34:14.61	–60:30:24.7	L	0.135	$<0.12$	-	-	$<-0.22$	-	-	
ATHDFS_J223440.4–603017	22:34:40.40	–60:30:17.7	L	0.226	-	-	-	-	-	-	
ATHDFS_J223216.6–603016	22:32:16.67	–60:30:16.7	L	0.052	(0.111)	-	-	$1.13 \pm 0.41$	-	-	AGN
ATHDFS_J223453.7–603008	22:34:53.72	–60:30:08.9	L	0.222	-	-	-	-	-	-	
ATHDFS_J223303.9–603013	22:33:03.96	–60:30:13.6	L	0.072	$<0.10$	(0.035)	$<0.12$	$<0.48$	-	-	
ATHDFS_J223203.6–603007	22:32:03.67	–60:30:07.0	L	0.380	-	-	-	-	-	-	
ATHDFS_J223331.1–603007	22:33:31.14	–60:30:07.9	L	0.107	$<0.09$	$<0.09$	-	$<-0.25$	-	-	
ATHDFS_J223430.1–602959	22:34:30.11	–60:29:59.4	L	0.441	0.280	-	-	$-0.50 \pm 0.21$	-	-	

Table 9—Continued

source name	RA	Dec	Coord Flag	$S_{1.4\text{GHz}}$	$S_{2.5\text{GHz}}$	$S_{5.2\text{GHz}}$	$S_{8.7\text{GHz}}$	$\alpha_{1.4\text{GHz}}^{2.5\text{GHz}}$	$\alpha_{2.5\text{GHz}}^{5.2\text{GHz}}$	$\alpha_{5.2\text{GHz}}^{8.7\text{GHz}}$	AGN flag
ATHDFS_J223236.5–603000	22:32:36.56	–60:30:00.6	L	1.507	0.877	0.446	-	$-0.86 \pm 0.05$	$-0.96 \pm 0.08$	-	
ATHDFS_J223224.7–603005	22:32:24.77	–60:30:05.5	L	0.055	<0.13	<0.09	-	<1.51	-	-	
ATHDFS_J223516.8–602959	22:35:16.84	–60:29:59.4	L	0.226	-	-	-	-	-	-	
ATHDFS_J223355.5–602956	22:33:55.54	–60:29:56.4	L	1.534	1.247	-	-	$-0.28 \pm 0.03$	-	-	AGN
ATHDFS_J223058.4–602952	22:30:58.48	–60:29:52.3	L	0.229	-	-	-	-	-	-	
ATHDFS_J223544.3–602950	22:35:44.33	–60:29:50.7	L	0.105	-	-	-	-	-	-	
ATHDFS_J223530.9–602951	22:35:30.90	–60:29:51.4	L	0.158	-	-	-	-	-	-	
ATHDFS_J223534.2–602948	22:35:34.20	–60:29:48.3	L	0.138	-	-	-	-	-	-	
ATHDFS_J223108.1–602946	22:31:08.17	–60:29:46.5	L	0.185	-	-	-	-	-	-	
ATHDFS_J223410.0–602949	22:34:10.03	–60:29:49.9	L	0.095	<0.13	-	-	<0.49	-	-	
ATHDFS_J223253.7–602946	22:32:53.78	–60:29:46.7	L	0.045	<0.10	(0.040)	<0.15	<1.36	-	-	
ATHDFS_J223316.8–602934	22:33:16.80	–60:29:34.7	C	1.003	0.811	0.569	-	$-0.16 \pm 0.06$	$-0.68 \pm 0.07$	-	AGN
ATHDFS_J223329.1–602933	22:33:29.16	–60:29:33.4	L	0.261	(0.122)	(0.068)	-	$-1.42 \pm 0.27$	$-0.43 \pm 0.29$	-	
ATHDFS_J223513.7–602930	22:35:13.71	–60:29:30.1	L	0.172	-	-	-	-	-	-	
ATHDFS_J223140.6–602924	22:31:40.62	–60:29:24.7	L	4.962	-	-	-	-	-	-	
ATHDFS_J223454.1–602926	22:34:54.16	–60:29:26.5	L	0.264	-	-	-	-	-	-	
ATHDFS_J223303.0–602927A	22:33:03.00	–60:29:27.1	L	0.116	<0.10	<0.07	-	<-0.22	-	-	
ATHDFS_J223303.0–602927B	22:33:01.82	–60:29:30.2	L	0.119	(0.049)	(0.055)	-	$-0.45 \pm 0.50$	$0.27 \pm 0.29$	-	
ATHDFS_J223415.3–602925	22:34:15.33	–60:29:25.5	L	0.291	(0.098)	-	-	$-1.50 \pm 0.27$	-	-	
ATHDFS_J223149.1–602924	22:31:49.11	–60:29:24.1	L	0.108	-	-	-	-	-	-	
ATHDFS_J223157.5–602919	22:31:57.53	–60:29:19.2	L	0.151	-	-	-	-	-	-	
ATHDFS_J223447.1–602915	22:34:47.11	–60:29:15.8	L	0.326	-	-	-	-	-	-	
ATHDFS_J223407.4–602913	22:34:07.43	–60:29:13.9	L	0.109	(0.078)	-	-	$0.02 \pm 0.32$	-	-	AGN
ATHDFS_J223317.7–602916	22:33:17.72	–60:29:16.0	L	0.068	<0.11	<0.08	-	<0.81	-	-	
ATHDFS_J223117.4–602850	22:31:17.48	–60:28:50.1	L	7.756	-	-	-	-	-	-	
ATHDFS_J223515.2–602856	22:35:15.23	–60:28:56.3	L	0.239	-	-	-	-	-	-	
ATHDFS_J223420.1–602901	22:34:20.14	–60:29:01.8	L	0.077	(0.116)	-	-	$1.47 \pm 0.45$	-	-	AGN
ATHDFS_J223445.3–602855	22:34:45.36	–60:28:55.8	L	0.276	-	-	-	-	-	-	
ATHDFS_J223431.7–602859	22:34:31.76	–60:28:59.5	L	0.071	-	-	-	-	-	-	
ATHDFS_J223212.1–602858	22:32:12.18	–60:28:58.4	L	0.124	-	-	-	-	-	-	
ATHDFS_J223505.0–602853	22:35:05.00	–60:28:53.4	L	0.187	-	-	-	-	-	-	
ATHDFS_J223236.2–602855	22:32:36.20	–60:28:55.6	L	0.094	<0.13	(0.053)	-	<0.58	-	-	
ATHDFS_J223108.3–602851	22:31:08.34	–60:28:51.6	L	0.086	-	-	-	-	-	-	
ATHDFS_J223307.7–602853	22:33:07.73	–60:28:53.8	L	0.068	(0.048)	<0.08	-	$-0.66 \pm 0.34$	-	-	
ATHDFS_J223127.7–602849	22:31:27.71	–60:28:49.2	L	0.120	-	-	-	-	-	-	
ATHDFS_J223326.9–602850	22:33:26.94	–60:28:50.0	L	0.182	(0.143)	-	-	$-0.64 \pm 0.27$	-	-	
ATHDFS_J223330.5–602849	22:33:30.55	–60:28:49.7	L	0.061	<0.12	-	-	<1.15	-	-	
ATHDFS_J223103.5–602830	22:31:03.51	–60:28:30.7	L	0.190	-	-	-	-	-	-	
ATHDFS_J223138.5–602834	22:31:38.51	–60:28:34.0	L	0.106	-	-	-	-	-	-	
ATHDFS_J223307.0–602827	22:33:07.07	–60:28:27.8	L	0.354	0.214	0.186	-	$-0.59 \pm 0.21$	$-0.25 \pm 0.29$	-	
ATHDFS_J223436.2–602821	22:34:36.23	–60:28:21.8	L	0.148	-	-	-	-	-	-	
ATHDFS_J223329.4–602811	22:33:29.40	–60:28:11.8	L	0.091	<0.11	-	-	<0.32	-	-	
ATHDFS_J223255.9–602810	22:32:55.99	–60:28:10.1	L	0.112	0.244	(0.076)	-	$1.55 \pm 0.31$	$-1.29 \pm 0.29$	-	GPS
ATHDFS_J223413.3–602808	22:34:13.30	–60:28:08.3	L	0.110	<0.14	-	-	<0.35	-	-	
ATHDFS_J223427.0–602802	22:34:27.02	–60:28:02.4	L	0.141	-	-	-	-	-	-	
ATHDFS_J223219.7–602802	22:32:19.73	–60:28:02.7	L	0.141	-	-	-	-	-	-	
ATHDFS_J223114.1–602800	22:31:14.13	–60:28:00.3	L	0.153	-	-	-	-	-	-	
ATHDFS_J223133.4–602755	22:31:33.40	–60:27:55.1	L	0.196	-	-	-	-	-	-	
ATHDFS_J223240.7–602755	22:32:40.71	–60:27:55.3	L	0.139	(0.069)	<0.12	-	$-1.03 \pm 0.32$	-	-	
ATHDFS_J223438.4–602747	22:34:38.40	–60:27:47.2	L	0.149	-	-	-	-	-	-	
ATHDFS_J223454.2–602742	22:34:54.23	–60:27:42.5	L	0.370	-	-	-	-	-	-	

Table 9—Continued

source name	RA	Dec	Coord Flag	$S_{1.4\text{GHz}}$	$S_{2.5\text{GHz}}$	$S_{5.2\text{GHz}}$	$S_{8.7\text{GHz}}$	$\alpha_{1.4\text{GHz}}^{2.5\text{GHz}}$	$\alpha_{2.5\text{GHz}}^{5.2\text{GHz}}$	$\alpha_{5.2\text{GHz}}^{8.7\text{GHz}}$	AGN flag
ATHDFS_J223443.9–602739A	22:34:43.99	–60:27:39.6	L	1.360	-	-	-	-	-	-	
ATHDFS_J223443.9–602739B	22:34:43.03	–60:27:34.4	L	1.221	-	-	-	-	-	-	
ATHDFS_J223443.9–602739C	22:34:42.01	–60:27:29.7	L	0.883	-	-	-	-	-	-	
ATHDFS_J223136.1–602731	22:31:36.13	–60:27:31.5	L	0.151	-	-	-	-	-	-	
ATHDFS_J223311.5–602725	22:33:11.53	–60:27:25.1	L	0.344	(0.161)	-	-	$-0.73 \pm 0.29$	-	-	
ATHDFS_J223142.7–602719	22:31:42.73	–60:27:19.6	L	0.338	-	-	-	-	-	-	
ATHDFS_J223153.1–602723	22:31:53.19	–60:27:23.3	L	0.119	-	-	-	-	-	-	
ATHDFS_J223148.6–602722	22:31:48.67	–60:27:22.0	L	0.132	-	-	-	-	-	-	
ATHDFS_J223332.7–602723	22:33:32.77	–60:27:23.5	L	0.087	<0.14	-	-	<0.76	-	-	
ATHDFS_J223241.5–602719	22:32:41.50	–60:27:19.8	L	0.391	-	-	-	-	-	-	
ATHDFS_J223227.6–602719A	22:32:27.60	–60:27:19.0	L	0.306	-	-	-	-	-	-	
ATHDFS_J223227.6–602719B	22:32:28.45	–60:27:10.0	L	0.108	-	-	-	-	-	-	
ATHDFS_J223418.3–602715	22:34:18.36	–60:27:15.6	L	0.196	-	-	-	-	-	-	
ATHDFS_J223244.5–602719	22:32:44.57	–60:27:19.2	L	0.103	<0.16	-	-	<0.71	-	-	
ATHDFS_J223317.1–602714	22:33:17.11	–60:27:14.1	L	0.122	(0.060)	-	-	$-1.30 \pm 0.34$	-	-	
ATHDFS_J223312.3–602707	22:33:12.30	–60:27:07.9	L	0.088	<0.15	-	-	<0.86	-	-	
ATHDFS_J223415.2–602701	22:34:15.26	–60:27:01.1	L	0.060	-	-	-	-	-	-	
ATHDFS_J223257.4–602657	22:32:57.44	–60:26:57.4	L	0.090	<0.15	-	-	<0.91	-	-	
ATHDFS_J223329.0–602657	22:33:29.08	–60:26:57.1	L	0.067	<0.13	-	-	<1.18	-	-	
ATHDFS_J223432.3–602652	22:34:32.34	–60:26:52.5	L	0.096	-	-	-	-	-	-	
ATHDFS_J223259.9–602654	22:32:59.93	–60:26:54.8	L	0.061	<0.15	-	-	<1.58	-	-	
ATHDFS_J223506.2–602647	22:35:06.28	–60:26:47.2	L	0.078	-	-	-	-	-	-	
ATHDFS_J223359.1–602642	22:33:59.14	–60:26:42.3	L	0.184	-	-	-	-	-	-	
ATHDFS_J223342.2–602639	22:33:42.23	–60:26:39.4	L	0.130	(0.090)	-	-	$-1.25 \pm 0.35$	-	-	
ATHDFS_J223221.4–602629	22:32:21.49	–60:26:29.7	L	4.274	-	-	-	-	-	-	
ATHDFS_J223400.9–602633	22:34:00.95	–60:26:33.6	L	0.097	-	-	-	-	-	-	
ATHDFS_J223212.4–602632	22:32:12.42	–60:26:32.2	L	0.143	-	-	-	-	-	-	
ATHDFS_J223136.2–602627	22:31:36.23	–60:26:27.6	L	0.150	-	-	-	-	-	-	
ATHDFS_J223432.6–602614	22:34:32.68	–60:26:14.3	L	0.318	-	-	-	-	-	-	
ATHDFS_J223335.3–602615	22:33:35.35	–60:26:15.0	L	0.172	(0.201)	-	-	$-0.06 \pm 0.29$	-	-	
ATHDFS_J223136.9–602610	22:31:36.98	–60:26:10.8	L	0.131	-	-	-	-	-	-	
ATHDFS_J223322.5–602607	22:33:22.57	–60:26:07.5	L	0.073	(0.083)	-	-	$0.17 \pm 0.44$	-	-	AGN
ATHDFS_J223442.5–602601	22:34:42.54	–60:26:01.4	L	0.056	-	-	-	-	-	-	
ATHDFS_J223307.2–602556	22:33:07.25	–60:25:56.5	L	0.234	-	-	-	-	-	-	
ATHDFS_J223148.3–602554	22:31:48.30	–60:25:54.0	L	0.210	-	-	-	-	-	-	
ATHDFS_J223357.8–602548	22:33:57.83	–60:25:48.0	L	0.164	-	-	-	-	-	-	
ATHDFS_J223308.8–602540	22:33:08.86	–60:25:40.6	L	0.095	-	-	-	-	-	-	
ATHDFS_J223202.6–602534	22:32:02.64	–60:25:34.5	L	0.174	-	-	-	-	-	-	
ATHDFS_J223222.4–602532	22:32:22.49	–60:25:32.3	L	0.105	-	-	-	-	-	-	
ATHDFS_J223432.2–602530	22:34:32.29	–60:25:30.1	L	0.074	-	-	-	-	-	-	
ATHDFS_J223445.7–602523	22:34:45.70	–60:25:23.1	L	0.181	-	-	-	-	-	-	
ATHDFS_J223351.2–602519	22:33:51.24	–60:25:19.6	L	0.103	-	-	-	-	-	-	
ATHDFS_J223141.1–602506	22:31:41.17	–60:25:06.6	L	0.301	-	-	-	-	-	-	
ATHDFS_J223228.9–602507	22:32:28.94	–60:25:07.9	L	0.164	-	-	-	-	-	-	
ATHDFS_J223134.5–602457	22:31:34.57	–60:24:57.4	L	0.416	-	-	-	-	-	-	
ATHDFS_J223306.6–602425	22:33:06.60	–60:24:25.9	L	1.949	-	-	-	-	-	-	
ATHDFS_J223317.1–602427	22:33:17.16	–60:24:27.6	L	0.232	-	-	-	-	-	-	
ATHDFS_J223444.9–602417	22:34:44.90	–60:24:17.1	L	9.581	-	-	-	-	-	-	
ATHDFS_J223436.8–602426	22:34:36.87	–60:24:26.8	L	0.128	-	-	-	-	-	-	
ATHDFS_J223245.3–602407	22:32:45.39	–60:24:07.7	L	0.469	-	-	-	-	-	-	
ATHDFS_J223343.4–602348	22:33:43.43	–60:23:48.8	L	0.111	-	-	-	-	-	-	

Table 9—Continued

source name	RA	Dec	Coord Flag	$S_{1.4\text{GHz}}$	$S_{2.5\text{GHz}}$	$S_{5.2\text{GHz}}$	$S_{8.7\text{GHz}}$	$\alpha_{1.4\text{GHz}}^{2.5\text{GHz}}$	$\alpha_{2.5\text{GHz}}^{5.2\text{GHz}}$	$\alpha_{5.2\text{GHz}}^{8.7\text{GHz}}$	AGN flag
ATHDFS_J223410.2–602324	22:34:10.27	–60:23:24.2	L	0.582	-	-	-	-	-	-	
ATHDFS_J223146.3–602313	22:31:46.37	–60:23:13.7	L	0.465	-	-	-	-	-	-	
ATHDFS_J223331.6–602307	22:33:31.68	–60:23:07.7	L	1.009	-	-	-	-	-	-	
ATHDFS_J223343.7–602307	22:33:43.76	–60:23:07.3	L	0.127	-	-	-	-	-	-	
ATHDFS_J223358.9–602258	22:33:58.90	–60:22:58.9	L	0.082	-	-	-	-	-	-	
ATHDFS_J223300.5–602225	22:33:00.57	–60:22:25.8	L	0.073	-	-	-	-	-	-	
ATHDFS_J223154.6–602211	22:31:54.67	–60:22:11.7	L	0.123	-	-	-	-	-	-	
ATHDFS_J223353.6–602136	22:33:53.69	–60:21:36.3	L	0.113	-	-	-	-	-	-	
ATHDFS_J223341.1–602054	22:33:41.11	–60:20:54.1	L	0.125	-	-	-	-	-	-	
ATHDFS_J223359.4–602047	22:33:59.46	–60:20:47.8	L	0.152	-	-	-	-	-	-	
ATHDFS_J223431.4–602041	22:34:31.48	–60:20:41.3	L	0.595	-	-	-	-	-	-	
ATHDFS_J223356.6–601949	22:33:56.68	–60:19:49.9	L	0.419	-	-	-	-	-	-	
ATHDFS_J223316.0–601939	22:33:16.02	–60:19:39.0	L	0.327	-	-	-	-	-	-	
ATHDFS_J223334.5–601928	22:33:34.53	–60:19:28.7	L	0.206	-	-	-	-	-	-	

flux density (1.4 GHz)	6.23 mJy
redshift $z$	0.65
log 1.4 GHz radio power ( $\text{W Hz}^{-1}$ )	25.0
V app mag	19.4
k corrected $M_V$	-25.6
linear extent	420 kpc

Table 10: Summary of broadline emitting radio galaxy ATHDFS\_223319.1-604428. The k-correction to  $M_V$  is from Pence (1976).

1.4 GHz integrated flux density	$16.4 \pm 1.2$ mJy
1.4 GHz integrated flux density (tapered image)	$21.0 \pm 1.5$ mJy
853 MHz integrated flux density	$16.3 \pm 1.4$ mJy
$\alpha_{853\text{MHz}}^{1.4\text{GHz}}$	$0.51 \pm 0.21$
redshift $z$	0.121
log 1.4 GHz radio power ( $\text{W Hz}^{-1}$ )	23.8
V app mag	16.31
k-corrected $M_V$	-22.6
U – B colour	0.38
B – V colour	1.37
V – R colour	0.68
R – I colour	0.68
linear extent	0.83 Mpc

Table 11: Summary of giant radio galaxy ATHDFS\_223432.9-601239. The k-correction to  $M_V$  is from Pence (1976).

name	$\alpha_{1.4\text{GHz}}^{2.5\text{GHz}}$
ATHDFS_J223408.1–604534	$-1.82 \pm 0.29$
ATHDFS_J223348.2–604026	$-1.25 \pm 0.35$
ATHDFS_J223343.7–603651	$-1.14 \pm 0.39$
ATHDFS_J223329.1–602933	$-1.42 \pm 0.27$

Table 12: High redshift AGN candidates selected using the ultra steep spectrum technique.



Table 13. Match data for the combined ATHDFS catalogue.

source name	1.4 GHz ID	2.5 GHz ID	5.2 GHz ID	8.7 GHz ID
ATHDFS_J223303.6–605751	1	-	-	-
ATHDFS_J223325.8–605729	2	-	-	-
ATHDFS_J223255.6–605656	3	-	-	-
ATHDFS_J223246.3–605654	4	-	-	-
ATHDFS_J223403.4–605640	5	-	-	-
ATHDFS_J223243.8–605608A	6	-	-	-
ATHDFS_J223243.8–605608B	7	-	-	-
ATHDFS_J223410.5–605545A	8	-	-	-
ATHDFS_J223410.5–605545B	9	-	-	-
ATHDFS_J223308.5–605544	10	-	-	-
ATHDFS_J223314.6–605543	11	-	-	-
ATHDFS_J223316.9–605533	12	-	-	-
ATHDFS_J223353.9–605452	13	-	-	-
ATHDFS_J223334.6–605455	14	-	-	-
ATHDFS_J223214.8–605430	15	-	-	-
ATHDFS_J223448.4–605417	16	-	-	-
ATHDFS_J223317.5–605416A	17	-	-	-
ATHDFS_J223317.5–605416B	18	-	-	-
ATHDFS_J223156.0–605417	19	-	-	-
ATHDFS_J223204.8–605414	20	-	-	-
ATHDFS_J223228.8–605406	21	-	-	-
ATHDFS_J223430.9–605357	22	-	-	-
ATHDFS_J223230.3–605352	23	-	-	-
ATHDFS_J223151.1–605328	24	-	-	-
ATHDFS_J223145.4–605311	25	-	-	-
ATHDFS_J223453.4–605259	26	-	-	-
ATHDFS_J223141.5–605302	27	-	-	-
ATHDFS_J223150.6–605258	28	-	-	-
ATHDFS_J223203.0–605242A	29	-	-	-
ATHDFS_J223203.0–605242B	30	-	-	-
ATHDFS_J223301.5–605250A	31	-	-	-
ATHDFS_J223301.5–605250B	32	-	-	-
ATHDFS_J223458.6–605225	33	-	-	-

Table 13—Continued

source name	1.4 GHz ID	2.5 GHz ID	5.2 GHz ID	8.7 GHz ID
ATHDFS_J223345.4–605227	34	-	-	-
ATHDFS_J223454.9–605211	35	-	-	-
ATHDFS_J223352.5–605210	36	-	-	-
ATHDFS_J223241.8–605209	37	-	-	-
ATHDFS_J223242.9–605155	38	-	-	-
ATHDFS_J223223.3–605137	39	-	-	-
ATHDFS_J223323.8–605141	40	-	-	-
ATHDFS_J223420.1–605138	41	-	-	-
ATHDFS_J223427.0–605132	42	-	-	-
ATHDFS_J223238.8–605113	43	-	-	-
ATHDFS_J223403.1–605101	44	-	-	-
ATHDFS_J223139.6–605039	45	-	-	-
ATHDFS_J223257.0–605039	46	-	-	-
ATHDFS_J223226.9–605029	47	-	-	-
ATHDFS_J223142.8–605024	48	-	-	-
ATHDFS_J223238.5–605018	49	-	-	-
ATHDFS_J223306.7–605014	50	-	-	-
ATHDFS_J223411.6–604931	51	-	-	-
ATHDFS_J223329.3–604931	52	-	-	-
ATHDFS_J223221.3–604929	53	-	-	-
ATHDFS_J223223.6–604923	54	-	-	-
ATHDFS_J223301.3–604926	55	-	-	-
ATHDFS_J223414.3–604923	56	-	-	-
ATHDFS_J223524.8–604918A	57	-	-	-
ATHDFS_J223524.8–604918B	58	-	-	-
ATHDFS_J223430.0–604922	59	-	-	-
ATHDFS_J223454.0–604904	60	-	-	-
ATHDFS_J223413.1–604909	61	-	-	-
ATHDFS_J223502.1–604858	62	-	-	-
ATHDFS_J223107.4–604855	63	-	-	-
ATHDFS_J223400.5–604903A	64	(72)	-	-
ATHDFS_J223400.5–604903B	65	-	-	-
ATHDFS_J223359.4–604901	66	-	-	-

Table 13—Continued

source name	1.4 GHz ID	2.5 GHz ID	5.2 GHz ID	8.7 GHz ID
ATHDFS_J223417.0–604857	67	-	-	-
ATHDFS_J223543.9–604838	68	-	-	-
ATHDFS_J223407.5–604847	69	(73)	-	-
ATHDFS_J223235.6–604844	70	-	-	-
ATHDFS_J223447.4–604843	71	-	-	-
ATHDFS_J223452.0–604834	72	-	-	-
ATHDFS_J223337.8–604833	73	(74)	-	-
ATHDFS_J223146.9–604827	74	-	-	-
ATHDFS_J223255.7–604823	75	(75)	-	-
ATHDFS_J223250.5–604814	76	-	-	-
ATHDFS_J223109.5–604810	77	-	-	-
ATHDFS_J223359.7–604806	78	(76)	-	-
ATHDFS_J223243.0–604758	79	(77)	-	-
ATHDFS_J223414.7–604753	80	(78)	-	-
ATHDFS_J223217.6–604751	81	-	-	-
ATHDFS_J223417.5–604749	82	-	-	-
ATHDFS_J223226.8–604745	83	1	-	-
ATHDFS_J223254.0–604736	84	2	-	-
ATHDFS_J223340.2–604730	85	-	-	-
ATHDFS_J223141.7–604725	86	-	-	-
ATHDFS_J223353.3–604723	87	-	-	-
ATHDFS_J223527.5–604714	88	-	-	-
ATHDFS_J223444.0–604710	89	-	-	-
ATHDFS_J223108.1–604706	90	-	-	-
ATHDFS_J223315.8–604707	91	-	-	-
ATHDFS_J223420.4–604658	92	-	-	-
ATHDFS_J223527.8–604639A	93	-	-	-
ATHDFS_J223527.8–604639B	94	-	-	-
ATHDFS_J223231.6–604654	95	-	-	-
ATHDFS_J223254.0–604650	96	-	-	-
ATHDFS_J223147.2–604647	97	-	-	-
ATHDFS_J223305.3–604647	98	-	-	-
ATHDFS_J223118.9–604644	99	-	-	-

Table 13—Continued

source name	1.4 GHz ID	2.5 GHz ID	5.2 GHz ID	8.7 GHz ID
ATHDFS_J223333.2–604642	100	3	-	-
ATHDFS_J223300.3–604640	101	-	-	-
ATHDFS_J223228.5–604642	102	-	-	-
ATHDFS_J223536.8–604632	103	-	-	-
ATHDFS_J223312.3–604630	104	-	-	-
ATHDFS_J223330.4–604624	105	(79)	-	-
ATHDFS_J223434.7–604603	106	(80)	-	-
ATHDFS_J223310.2–604601	107	-	-	-
ATHDFS_J223258.6–604548	108	-	-	-
ATHDFS_J223329.6–604537	109	4	-	-
ATHDFS_J223408.1–604534	110	(81)	-	-
ATHDFS_J223342.9–604524	111	5	-	-
ATHDFS_J223324.0–604516	112	-	-	-
ATHDFS_J223320.1–604457	113	-	-	-
ATHDFS_J223443.3–604452	114	6	-	-
ATHDFS_J223121.4–604448	115	-	-	-
ATHDFS_J223311.5–604449	116	(82)	-	-
ATHDFS_J223319.1–604428	117	8	-	-
ATHDFS_J223210.3–604433	118	7	-	-
ATHDFS_J223439.0–604435	119	(84)	-	-
ATHDFS_J223356.9–604438	120	-	-	-
ATHDFS_J223244.1–604437	121	(83)	-	-
ATHDFS_J223147.2–604415	122	-	-	-
ATHDFS_J223326.3–604416	123	-	-	-
ATHDFS_J223255.2–604415	124	-	-	-
ATHDFS_J223422.4–604412	125	(85)	-	-
ATHDFS_J223226.8–604408	126	-	-	-
ATHDFS_J223313.9–604359	127	-	-	-
ATHDFS_J223255.6–604400	128	9	-	-
ATHDFS_J223101.3–604351	129	-	-	-
ATHDFS_J223319.1–604348	130	10	-	-
ATHDFS_J223147.4–604338	131	-	-	-
ATHDFS_J223126.2–604337	132	-	-	-

Table 13—Continued

source name	1.4 GHz ID	2.5 GHz ID	5.2 GHz ID	8.7 GHz ID
ATHDFS_J223439.7–604337	133	-	-	-
ATHDFS_J223534.3–604328	134	-	-	-
ATHDFS_J223250.6–604336	135	-	-	-
ATHDFS_J223522.2–604326	136	-	-	-
ATHDFS_J223330.4–604332	137	-	-	-
ATHDFS_J223355.6–604315	138	11	-	-
ATHDFS_J223440.4–604309	139	-	-	-
ATHDFS_J223430.8–604310	140	-	-	-
ATHDFS_J223240.2–604306	141	(86)	-	-
ATHDFS_J223207.9–604305	142	-	-	-
ATHDFS_J223427.3–604258	143	12	-	-
ATHDFS_J223130.4–604232	144	-	-	-
ATHDFS_J223425.8–604232	145	(87)	-	-
ATHDFS_J223239.0–604230	146	-	-	-
ATHDFS_J223312.4–604227	147	13	-	-
ATHDFS_J223437.2–604214	148	14	-	-
ATHDFS_J223508.5–604217	149	-	-	-
ATHDFS_J223338.8–604216	150	15	-	-
ATHDFS_J223523.6–604207	151	-	-	-
ATHDFS_J223135.8–604207	152	-	-	-
ATHDFS_J223359.8–604155	153	16	-	-
ATHDFS_J223255.4–604151	154	(88)	-	-
ATHDFS_J223158.4–604142	155	-	-	-
ATHDFS_J223339.5–604131	156	(89)	-	-
ATHDFS_J223224.5–604113	157	17	-	-
ATHDFS_J223206.5–604102	158	-	-	-
ATHDFS_J223448.3–604042	159	18	-	-
ATHDFS_J223430.1–604043	160	-	-	-
ATHDFS_J223251.1–604042	161	-	-	-
ATHDFS_J223514.4–604024	162	-	-	-
ATHDFS_J223348.2–604026	163	(90)	-	-
ATHDFS_J223429.8–604020	164	(91)	-	-
ATHDFS_J223417.8–604009	165	19	-	-

Table 13—Continued

source name	1.4 GHz ID	2.5 GHz ID	5.2 GHz ID	8.7 GHz ID
ATHDFS_J223337.5–604006	166	-	-	-
ATHDFS_J223412.2–603957	167	-	-	-
ATHDFS_J223438.0–603951	168	(92)	-	-
ATHDFS_J223343.9–603953	169	-	-	-
ATHDFS_J223047.9–603933	170	-	-	-
ATHDFS_J223324.7–603934	171	(93)	-	-
ATHDFS_J223220.6–603931	172	20	-	-
ATHDFS_J223529.2–603927	173	-	-	-
ATHDFS_J223400.2–603930	174	-	-	-
ATHDFS_J223207.9–603928	175	(94)	-	-
ATHDFS_J223222.7–603924	176	-	-	-
ATHDFS_J223253.7–603921	177	-	-	-
ATHDFS_J223331.3–603914	178	-	-	-
ATHDFS_J223123.1–603903	179	-	-	-
ATHDFS_J223258.7–603903	180	(95)	-	-
ATHDFS_J223245.6–603857	181	21	-	-
ATHDFS_J223205.9–603857	182	22	-	-
ATHDFS_J223144.4–603858	183	-	-	-
ATHDFS_J223153.7–603853	184	-	-	-
ATHDFS_J223450.4–603844	185	(97)	-	-
ATHDFS_J223307.1–603846	186	23	-	-
ATHDFS_J223457.3–603840	187	(96)	-	-
ATHDFS_J223232.3–603842	188	(98)	-	-
ATHDFS_J223335.9–603828	-	24	-	-
ATHDFS_J223505.5–603825	189	-	-	-
ATHDFS_J223304.6–603835	190	-	-	-
ATHDFS_J223608.1–603823	191	-	-	-
ATHDFS_J223432.1–603815	192	25	-	-
ATHDFS_J223138.7–603818	193	-	-	-
ATHDFS_J223418.6–603808	194	26	-	-
ATHDFS_J223442.7–603802	195	27	-	-
ATHDFS_J223248.2–603805	196	(99)	-	-
ATHDFS_J223334.4–603804	197	-	-	-

Table 13—Continued

source name	1.4 GHz ID	2.5 GHz ID	5.2 GHz ID	8.7 GHz ID
ATHDFS_J223436.9–603754	198	28	-	-
ATHDFS_J223346.9–603753	-	29	-	-
ATHDFS_J223254.5–603748	199	-	-	-
ATHDFS_J223350.0–603741	200	30,31	-	-
ATHDFS_J223441.6–603740	201	(100)	-	-
ATHDFS_J223232.8–603737	202	32	1	-
ATHDFS_J223142.5–603737	203	-	-	-
ATHDFS_J223404.8–603732	204	33	-	-
ATHDFS_J223503.2–603729	205	-	-	-
ATHDFS_J223437.7–603726	206	(101)	-	-
ATHDFS_J223417.1–603724	207	(102)	-	-
ATHDFS_J223341.2–603724	208	(103)	-	-
ATHDFS_J223225.6–603717	209	-	-	-
ATHDFS_J223202.5–603714	210	(104)	-	-
ATHDFS_J223326.0–603716	211	-	-	-
ATHDFS_J223506.5–603700	212	-	-	-
ATHDFS_J223236.6–603657	-	34	-	-
ATHDFS_J223400.2–603653	213	35	-	-
ATHDFS_J223525.8–603652	214	-	-	-
ATHDFS_J223343.7–603651	215	(105)	-	-
ATHDFS_J223404.3–603638	216	36	-	-
ATHDFS_J223158.1–603636	217	(107)	-	-
ATHDFS_J223605.7–603631	218	-	-	-
ATHDFS_J223406.7–603637	219	(106)	-	-
ATHDFS_J223054.4–603631	220	-	-	-
ATHDFS_J223439.9–603629	221	-	-	-
ATHDFS_J223341.9–603634	222	(109)	-	-
ATHDFS_J223451.7–603632	223	(108)	-	-
ATHDFS_J223429.9–603629	224	37	-	-
ATHDFS_J223316.5–603627	225	38	2	-
ATHDFS_J223526.2–603617	226	-	-	-
ATHDFS_J223518.7–603619	227	-	-	-
ATHDFS_J223456.2–603619	228	(110)	-	-

Table 13—Continued

source name	1.4 GHz ID	2.5 GHz ID	5.2 GHz ID	8.7 GHz ID
ATHDFS_J223158.5–603614	229	-	-	-
ATHDFS_J223410.3–603613	230	-	-	-
ATHDFS_J223421.8–603603	231	-	-	-
ATHDFS_J223232.4–603542A	232	39	4	-
ATHDFS_J223232.4–603542B	233	40	3	-
ATHDFS_J223104.8–603549	234	-	-	-
ATHDFS_J223525.7–603544	235	-	-	-
ATHDFS_J223229.8–603544	236	(111)	-	-
ATHDFS_J223422.0–603544	-	48	-	-
ATHDFS_J223224.0–603537	237	41	5	-
ATHDFS_J223253.0–603539	238	(112)	(25)	-
ATHDFS_J223459.4–603535	239	-	-	-
ATHDFS_J223245.3–603537	240	-	-	-
ATHDFS_J223046.1–603525	241	-	-	-
ATHDFS_J223435.5–603532	242	(113)	-	-
ATHDFS_J223338.8–603523	243	42	-	-
ATHDFS_J223208.3–603519	244	43	-	-
ATHDFS_J223223.7–603520	245	-	-	-
ATHDFS_J223344.9–603515	246	44	-	-
ATHDFS_J223524.8–603509	247	-	-	-
ATHDFS_J223536.3–603506	248	-	-	-
ATHDFS_J223410.1–603510	249	45	-	-
ATHDFS_J223549.5–603502	250	-	-	-
ATHDFS_J223350.5–603503	251	46	-	-
ATHDFS_J223229.2–603459A	252	(114)	(26)	-
ATHDFS_J223229.2–603459B	253	47	6	-
ATHDFS_J223541.5–603454	254	-	-	-
ATHDFS_J223438.6–603450	255	48	-	-
ATHDFS_J223103.2–603453	256	-	-	-
ATHDFS_J223116.4–603452	257	-	-	-
ATHDFS_J223431.8–603454	258	(115)	-	-
ATHDFS_J223425.0–603452	259	(116)	-	-
ATHDFS_J223212.3–603448	260	-	-	-



Table 13—Continued

source name	1.4 GHz ID	2.5 GHz ID	5.2 GHz ID	8.7 GHz ID
ATHDFS_J223307.1–603448	261	-	-	-
ATHDFS_J223207.4–603445	262	-	-	-
ATHDFS_J223243.3–603443	263	-	7	-
ATHDFS_J223410.6–603437	264	-	-	-
ATHDFS_J223442.8–603433	265	-	-	-
ATHDFS_J223216.6–603434	266	-	-	-
ATHDFS_J223539.3–603424	267	-	-	-
ATHDFS_J223153.2–603422	268	(118)	-	-
ATHDFS_J223401.0–603424	269	(117)	-	-
ATHDFS_J223245.5–603419	270	49	8	(7)
ATHDFS_J223231.6–603423	271	-	(27)	-
ATHDFS_J223055.9–603412	272	-	-	-
ATHDFS_J223327.6–603414	273	50	9	-
ATHDFS_J223311.9–603417	274	(119)	(28)	-
ATHDFS_J223434.1–603410	275	(120)	-	-
ATHDFS_J223053.2–603402	276	-	-	-
ATHDFS_J223415.0–603408	277	-	-	-
ATHDFS_J223529.7–603359	278	-	-	-
ATHDFS_J223406.6–603401	279	-	-	-
ATHDFS_J223409.7–603402	280	-	-	-
ATHDFS_J223512.7–603353	281	-	-	-
ATHDFS_J223306.0–603350	282	51	12	(8)
ATHDFS_J223329.7–603352	283	52	10	-
ATHDFS_J223258.5–603346	284	53	13	2
ATHDFS_J223243.4–603352	285	(121)	11	1
ATHDFS_J223545.7–603342	286	-	-	-
ATHDFS_J223138.5–603344	287	-	-	-
ATHDFS_J223420.9–603336	288	54	-	-
ATHDFS_J223225.0–603338	289	-	-	-
ATHDFS_J223513.7–603333	290	-	-	-
ATHDFS_J223247.6–603337	291	-	(29)	-
ATHDFS_J223337.5–603329	292	55	14	-
ATHDFS_J223253.1–603329	293	(122)	-	-

Table 13—Continued

source name	1.4 GHz ID	2.5 GHz ID	5.2 GHz ID	8.7 GHz ID
ATHDFS_J223302.8–603323	294	-	-	-
ATHDFS_J223509.5–603257	295	-	-	-
ATHDFS_J223327.9–603304A	296	56	15	-
ATHDFS_J223327.9–603304B	297	-	-	-
ATHDFS_J223306.2–603307	-	-	-	3
ATHDFS_J223339.4–603306	298	-	-	-
ATHDFS_J223121.6–603301	299	-	-	-
ATHDFS_J223242.6–603258	-	-	-	4
ATHDFS_J223234.2–603257	300	-	-	-
ATHDFS_J223308.6–603251	301	57,58	16	5
ATHDFS_J223456.8–603251	302	-	-	-
ATHDFS_J223323.2–603249	303	59	17	6
ATHDFS_J223209.7–603253	304	-	-	-
ATHDFS_J223212.9–603234A	305	60	20	-
ATHDFS_J223212.9–603234B	306	61	18	-
ATHDFS_J223229.5–603243	307	62	19	-
ATHDFS_J223509.4–603235	308	-	-	-
ATHDFS_J223142.5–603238	309	-	-	-
ATHDFS_J223521.1–603235	310	-	-	-
ATHDFS_J223317.7–603235	311	-	(30)	-
ATHDFS_J223335.3–603234	312	-	-	-
ATHDFS_J223429.9–603226	313	-	-	-
ATHDFS_J223331.6–603222	314	63	21	-
ATHDFS_J223504.4–603221	315	-	-	-
ATHDFS_J223343.5–603211	316	-	-	-
ATHDFS_J223302.1–603213	317	-	-	-
ATHDFS_J223519.4–603157A	318	-	-	-
ATHDFS_J223519.4–603157B	319	-	-	-
ATHDFS_J223351.1–603153	-	64	-	-
ATHDFS_J223113.5–603147	320	-	-	-
ATHDFS_J223433.9–603150	321	-	-	-
ATHDFS_J223449.7–603137	322	-	-	-
ATHDFS_J223303.1–603132	323	(123)	(31)	-

Table 13—Continued

source name	1.4 GHz ID	2.5 GHz ID	5.2 GHz ID	8.7 GHz ID
ATHDFS_J223254.4–603131	324	(124)	(32)	-
ATHDFS_J223316.0–603127	325	-	(33)	-
ATHDFS_J223548.9–603113	326	-	-	-
ATHDFS_J223201.4–603118	327	-	-	-
ATHDFS_J223351.7–603117	328	(125)	-	-
ATHDFS_J223504.6–603109	329	-	-	-
ATHDFS_J223415.5–603108	330	-	-	-
ATHDFS_J223256.4–603058	331	-	(34)	-
ATHDFS_J223550.9–603050	332	-	-	-
ATHDFS_J223447.4–603050	333	-	-	-
ATHDFS_J223146.0–603046	334	-	-	-
ATHDFS_J223345.0–603041	335	(126)	-	-
ATHDFS_J223404.0–603037A	336	65	-	-
ATHDFS_J223404.0–603037B	337	(127)	-	-
ATHDFS_J223445.6–603032	338	-	-	-
ATHDFS_J223304.8–603031	339	-	(35)	-
ATHDFS_J223120.1–603025	340	-	-	-
ATHDFS_J223537.7–603013	341	-	-	-
ATHDFS_J223241.4–603025	342	(128)	(36)	-
ATHDFS_J223414.6–603024	343	-	-	-
ATHDFS_J223440.4–603017	344	-	-	-
ATHDFS_J223216.6–603016	345	(129)	-	-
ATHDFS_J223453.7–603008	346	-	-	-
ATHDFS_J223303.9–603013	347	-	(37)	-
ATHDFS_J223203.6–603007	348	-	-	-
ATHDFS_J223331.1–603007	349	-	-	-
ATHDFS_J223430.1–602959	350	67	-	-
ATHDFS_J223236.5–603000	351	66	22	-
ATHDFS_J223224.7–603005	352	-	-	-
ATHDFS_J223516.8–602959	353	-	-	-
ATHDFS_J223355.5–602956	354	68	-	-
ATHDFS_J223058.4–602952	355	-	-	-
ATHDFS_J223544.3–602950	356	-	-	-

Table 13—Continued

source name	1.4 GHz ID	2.5 GHz ID	5.2 GHz ID	8.7 GHz ID
ATHDFS_J223530.9–602951	357	-	-	-
ATHDFS_J223534.2–602948	358	-	-	-
ATHDFS_J223108.1–602946	359	-	-	-
ATHDFS_J223410.0–602949	360	-	-	-
ATHDFS_J223253.7–602946	361	-	(38)	-
ATHDFS_J223316.8–602934	362	69	23	-
ATHDFS_J223329.1–602933	363	(130)	(39)	-
ATHDFS_J223513.7–602930	364	-	-	-
ATHDFS_J223140.6–602924	365	-	-	-
ATHDFS_J223454.1–602926	366	-	-	-
ATHDFS_J223303.0–602927A	367	-	-	-
ATHDFS_J223303.0–602927B	368	(131)	(40)	-
ATHDFS_J223415.3–602925	369	(132)	-	-
ATHDFS_J223149.1–602924	370	-	-	-
ATHDFS_J223157.5–602919	371	-	-	-
ATHDFS_J223447.1–602915	372	-	-	-
ATHDFS_J223407.4–602913	373	(133)	-	-
ATHDFS_J223317.7–602916	374	-	-	-
ATHDFS_J223117.4–602850	375	-	-	-
ATHDFS_J223515.2–602856	376	-	-	-
ATHDFS_J223420.1–602901	377	(134)	-	-
ATHDFS_J223445.3–602855	378	-	-	-
ATHDFS_J223431.7–602859	379	-	-	-
ATHDFS_J223212.1–602858	380	-	-	-
ATHDFS_J223505.0–602853	381	-	-	-
ATHDFS_J223236.2–602855	382	-	(41)	-
ATHDFS_J223108.3–602851	383	-	-	-
ATHDFS_J223307.7–602853	384	(135)	-	-
ATHDFS_J223127.7–602849	385	-	-	-
ATHDFS_J223326.9–602850	386	(136)	-	-
ATHDFS_J223330.5–602849	387	-	-	-
ATHDFS_J223103.5–602830	388	-	-	-
ATHDFS_J223138.5–602834	389	-	-	-

Table 13—Continued

source name	1.4 GHz ID	2.5 GHz ID	5.2 GHz ID	8.7 GHz ID
ATHDFS_J223307.0–602827	390	70	24	-
ATHDFS_J223436.2–602821	391	-	-	-
ATHDFS_J223329.4–602811	392	-	-	-
ATHDFS_J223255.9–602810	393	71	(42)	-
ATHDFS_J223413.3–602808	394	-	-	-
ATHDFS_J223427.0–602802	395	-	-	-
ATHDFS_J223219.7–602802	396	-	-	-
ATHDFS_J223114.1–602800	397	-	-	-
ATHDFS_J223133.4–602755	398	-	-	-
ATHDFS_J223240.7–602755	399	(137)	-	-
ATHDFS_J223438.4–602747	400	-	-	-
ATHDFS_J223454.2–602742	401	-	-	-
ATHDFS_J223443.9–602739A	402	-	-	-
ATHDFS_J223443.9–602739B	403	-	-	-
ATHDFS_J223443.9–602739C	404	-	-	-
ATHDFS_J223136.1–602731	405	-	-	-
ATHDFS_J223311.5–602725	406	(138)	-	-
ATHDFS_J223142.7–602719	407	-	-	-
ATHDFS_J223153.1–602723	408	-	-	-
ATHDFS_J223148.6–602722	409	-	-	-
ATHDFS_J223332.7–602723	410	-	-	-
ATHDFS_J223241.5–602719	411	-	-	-
ATHDFS_J223227.6–602719A	412	-	-	-
ATHDFS_J223227.6–602719B	413	-	-	-
ATHDFS_J223418.3–602715	414	-	-	-
ATHDFS_J223244.5–602719	415	-	-	-
ATHDFS_J223317.1–602714	416	(139)	-	-
ATHDFS_J223312.3–602707	417	-	-	-
ATHDFS_J223415.2–602701	418	-	-	-
ATHDFS_J223257.4–602657	419	-	-	-
ATHDFS_J223329.0–602657	420	-	-	-
ATHDFS_J223432.3–602652	421	-	-	-
ATHDFS_J223259.9–602654	422	-	-	-

Table 13—Continued

source name	1.4 GHz ID	2.5 GHz ID	5.2 GHz ID	8.7 GHz ID
ATHDFS_J223506.2–602647	423	-	-	-
ATHDFS_J223359.1–602642	424	-	-	-
ATHDFS_J223342.2–602639	425	(140)	-	-
ATHDFS_J223221.4–602629	426	-	-	-
ATHDFS_J223400.9–602633	427	-	-	-
ATHDFS_J223212.4–602632	428	-	-	-
ATHDFS_J223136.2–602627	429	-	-	-
ATHDFS_J223432.6–602614	430	-	-	-
ATHDFS_J223335.3–602615	431	(141)	-	-
ATHDFS_J223136.9–602610	432	-	-	-
ATHDFS_J223322.5–602607	433	(142)	-	-
ATHDFS_J223442.5–602601	434	-	-	-
ATHDFS_J223307.2–602556	435	-	-	-
ATHDFS_J223148.3–602554	436	-	-	-
ATHDFS_J223357.8–602548	437	-	-	-
ATHDFS_J223308.8–602540	438	-	-	-
ATHDFS_J223202.6–602534	439	-	-	-
ATHDFS_J223222.4–602532	440	-	-	-
ATHDFS_J223432.2–602530	441	-	-	-
ATHDFS_J223445.7–602523	442	-	-	-
ATHDFS_J223351.2–602519	443	-	-	-
ATHDFS_J223141.1–602506	444	-	-	-
ATHDFS_J223228.9–602507	445	-	-	-
ATHDFS_J223134.5–602457	446	-	-	-
ATHDFS_J223306.6–602425	447	-	-	-
ATHDFS_J223317.1–602427	448	-	-	-
ATHDFS_J223444.9–602417	449	-	-	-
ATHDFS_J223436.8–602426	450	-	-	-
ATHDFS_J223245.3–602407	451	-	-	-
ATHDFS_J223343.4–602348	452	-	-	-
ATHDFS_J223410.2–602324	453	-	-	-
ATHDFS_J223146.3–602313	454	-	-	-
ATHDFS_J223331.6–602307	455	-	-	-

Table 13—Continued

source name	1.4 GHz ID	2.5 GHz ID	5.2 GHz ID	8.7 GHz ID
ATHDFS_J223343.7–602307	456	-	-	-
ATHDFS_J223358.9–602258	457	-	-	-
ATHDFS_J223300.5–602225	458	-	-	-
ATHDFS_J223154.6–602211	459	-	-	-
ATHDFS_J223353.6–602136	460	-	-	-
ATHDFS_J223341.1–602054	461	-	-	-
ATHDFS_J223359.4–602047	462	-	-	-
ATHDFS_J223431.4–602041	463	-	-	-
ATHDFS_J223356.6–601949	464	-	-	-
ATHDFS_J223316.0–601939	465	-	-	-
ATHDFS_J223334.5–601928	466	-	-	-